The Van der Waal's Endpoint Problem and the Treatment of Long-Range Interactions in Free Energy Difference Simulations

DIPLOMARBEIT

eingereicht von

Michael Brunsteiner

zur Erlangung des akademischen Grades

Diplom Ingenieur

an der Universität für Bodenkultur, Wien

Dezember 1999

Danksagung

Ich möchte mich bedanken ...

bei meinen Betreuern und Lehrern, Prof J. Fischer und Prof. O. Steinhauser für die Ressourcen, die sie mir großzügig zur Verfügung stellten und insbesondere bei Dr. Stefan Boresch für seine intensive und kompetente Betreuung.

bei meinen Eltern (allen Dreien) sowie bei meinen Großeltern für ihre ausdauernde seelische sowie finanzielle Unterstützung und die aussergewöhnliche Geduld, die sie dabei bewiesen.

Zusammenfassung

Thema dieser Arbeit ist die Berechnung freier Energiedifferenzen mithilfe von Molekular-Dynamik Computersimulationen. Im Gegensatz zur experimentellen Bestimmung dieser Größen, kann diese Herangehensweise die Möglichkeit eines detailierten Einblicks in die molekularen Grundlagen freier Energiedifferenzen verschaffen. Mögliche Anwendungen umfassen die Bestimmung von relativen Affinitäten zwischen Rezeptoren und verschiedenen Liganden, der Sequenzabhängigen Stabilität von Proteinen, von Gleichgewichts-Koeffizienten in nicht-wässrigen Lösungen etc.

Spezielles Augenmerk wurde gerichtet auf zweierlei Probleme, die bei solchen Rechnungen auftreten können: das sogenannte *Van der Waal's endpoint problem* und die konsistente Behandlung elektrostatischen Wechselwirkungen im Rahmen solcher Rechnungen. *Separation Shifted Scaling*, eine numerische Methode zur Lösung des *Van der Waal's endpoint problem* wurde in CHARMM, einem gängigen Molekular-dynamik Programm-Paket implementiert. Es konnte gezeigt werden, daß die Methode nicht nur in der Lage ist, das *Van der Waal's endpoint problem* zu lösen, sondern dies auch mit, im Vergleich zu anderen Methoden grösserer Effizienz bewerkstelligt. Ferner konnte gezeigt werden, daß die Resultate von Berechnungen der freien Energie-Differenzen von polaren Molekülen sehr empfindlich von Art der Behandlung weitreichender, i.e, elektrostaischer und Dipol-Dipol-Wechselwirkungen abhängt und daß im Regelfall die Verwendung vergleichsweise aufwendiger Methoden zur Berechnung der coulombschen Wechselwirkungen, wie z.B. der Ewald-Summation, angebracht ist.

Abstract

Separation Shifted Scaling, a computational method coping with the Van der Waal's endpoint problem in free energy simulations, was implemented in the MD-package CHARMM. Test-calculations were carried out for various systems to verify the correctness of the computer code. The free energies of hydration of neon, as well as of water, were calculated using thermodynamic integration in combination with the separation shifted potential for Van der Waal's and Coulomb interactions. The method proved to be very efficient and yielded results with good precision.

The calculations for water were repeated for different sizes of the simulation system and cutoff radii in combination with different methods to handle the long range interactions. Results obtained with Ewald-summation, several tapering functions and a generalized reaction field potential were compared. Results obtained with Ewald summation were independent of system size. Thus they were used as reference values. The other free energy results turned out to depend sensitively on the cutoff-radius and on the method treatment of the long range interactions. A cutoff larger than 12 Å has to be used to get results independent of the choice of the tapering function. Only group based switching of the Coulomb interactions with electrically neutral groups yielded results independent of the cutoff-radius.

Contents

1 Introduction

More than forty years ago Metropolis et. al[1] invented the Monte Carlo (MC) method, and Alder and Wainwright[2] performed the first molecular dynamics (MD) simulations of hard spheres. Since then numerous variations of these two methods have been used in a wide range of *computer experiments* to probe the laws determining the structure and properties of matter.

The focus of many, if not most computer simulation studies has been the liquid state. For liquids the comparatively simple rules found to describe solids and gases break down and have to be replaced by considerably more complicated descriptions and/or less accurate approximations. Computer simulation of molecular ensembles is a useful tool for studying the validity of theoretical concepts in this area. It allows the analysis and — in the best case — the understanding of a macroscopic property or dynamical process on a molecular scale.

In the context of MD the classical equations of motion for a microscopic sample of molecules are solved by numerical integration — resulting in a sequence of coordinates and velocities. The connection between these data and macroscopic quantities, such as pressure and temperature, is provided by statistical mechanics. Strictly speaking the equations of statistical mechanics are valid only in the thermodynamic limit, i.e., for the number of particles $N \to \infty$. It turns out, however, that in many cases a simulation of a few hundred molecules can already recover a number of useful thermodynamic and structural properties of a particular substance.

A quite prominent place in every textbook on statistical mechanics is usually occupied by the various thermodynamic potentials. The Helmholtz and the Gibbs free energy, as opposed to the internal energy or enthalpy, are of a special interest since knowing their values for different states of a particular system allows one to make predictions for the relative stability of these states. Although demanding in terms of CPU-power, free energy differences are among the quantities that can

be obtained from computer simulations. Because of the steep rise in computer performance such free energy simulations have become a valuable tool complementing experimental measurements. Examples for possible applications are the calculation of relative receptor-ligand binding affinities, protein stability, solvation and partition coefficients. Although it can be considered a standard method by now, there still are quite a few problems and pitfalls one can encounter when calculating free energy differences by MD. Some of these problems and attempts to their solution, respectively, are the subject of this thesis. (i) A rather new algorithm (*Separation Shifted Scaling* [3, 4] (SSS)) developed to circumvent the so-called Van der Waals-endpoint-problem, is discussed. As a part of the thesis this algorithm was implemented into the well known MD-package CHARMM [5]. Calculations were carried out to test its usefulness and applicability. The results were compared to data found in the literature as well as to results obtained with a method already implemented in CHARMM. (ii) Further, the generalized reaction field (GRF) potential [6] — a special method for dealing with the long range nature of the coulomb interactions — was implemented into CHARMM. During the analysis of the gathered free energy data special attention was directed to the impact which different ways to handle the electrostatic interactions had on the results.

This masters thesis is organized as follows: In chapter 2 the fundamental concepts and equations describing free energy and related quantities are presented, followed by a brief outline of the common methods used for the calculation of free energies by computer simulations. Some of the problems arising in such calculations and different approaches for their solution, including SSS, are presented and discussed. The chapter is concluded by a short introduction into the problem of the consistent treatment of long range interactions. In Chapter 3 the actual implementation of SSS, as well as the GRF-potential, into CHARMM are described. Technical details of the computer simulations and of the test-systems, (force field parameters etc.) are given in chapter 4. The first part of section 5 presents the

results of the test calculations for different algorithms, while in the second part the findings concerning the influence of the handling of the long range interactions are presented. Chapter 6 finally gives a summary and concluding discussion.

2 Theory

2.1 Statistical Mechanics

For a more detailed account of the theoretical background the reader is referred to appropriate textbooks [7, 8]. Here merely some definitions of statistical mechanical quantities are given beforehand. Apart from some hybrid approaches molecular dynamics simulations are usually a completely classical method. Therefore all the derivations given in this section are valid only in the realm of classical statistical mechanics*.

Within the framework of phenomenological thermodynamics the Helmholtz free energy A — henceforth just called free energy — is defined as a Legendre transform of U, the internal energy, A = U - T S — S and T being the entropy and temperature, respectively. Within statistical mechanics A is given by,

$$A = -k_{\mathrm{B}} T \ln Q, \tag{1}$$

where k_{B} is the Boltzmann constant and Q is the canonical partition function. For a system with Hamilatonian $\mathcal{H}$, constant volume V, constant temperature T and constant number of particles N, Q is given in the classical limit as a function of the momenta $\{\vec{p}_1, \vec{p}_2, ..., \vec{p}_n\} \equiv \mathbf{p}$ and coordinates $\{\vec{r}_1, \vec{r}_2, ..., \vec{r}_n\} \equiv \mathbf{x}$ of all particles integrated over the whole phase space

$$Q = \frac{1}{N! h^{3N}} \int_{-\infty}^{\infty} \int_{V} \exp\left(-\beta \mathcal{H}(\mathbf{x}, \mathbf{p})\right) d\mathbf{x} d\mathbf{p} \tag{2}$$

*Apart of course from relations that are valid in both, i.e., the classical and the quantum mechanical realms

As usual $\beta = 1/k_{\mathrm{B}}T$. The free energy, as expressed in equation 1 provides the essential link between statistical mechanics and classical thermodynamics, i.e. between the macroscopic quantity A and the microscopic quantities $\mathbf{x}$ and $\mathbf{p}$. Starting with equation 1, it is possible to derive expressions for all the thermodynamic functions in terms of Q.

The probability P to find the system at a particular point in phase space defined by the coordinates $\mathbf{x}$ and the momenta $\mathbf{p}$ is given by

$$P(\mathbf{x},\mathbf{p}) = \frac{1}{Q}\exp\left(-\beta\mathcal{H}(\mathbf{x},\mathbf{p})\right) \tag{3}$$

The expectation value $\langle X\rangle$ for some property $X(\mathbf{x},\mathbf{p})$ is the ensemble average

$$\langle X\rangle = \int_{-\infty}^{\infty}\int_{V} X(\mathbf{x},\mathbf{p})P(\mathbf{x},\mathbf{p})d\mathbf{x}d\mathbf{p} \tag{4}$$

If the Hamiltonian of the system can be divided into a part that depends only on the momenta, and another part that depends only on the coordinates, i.e., if $\mathcal{H}(\mathbf{x},\mathbf{p}) = \mathcal{T}(\mathbf{p}) + \mathcal{V}(\mathbf{x})$, then the expectation value of a property X($\mathbf{x}$), which is also a function of the coordinates only, can be found from

$$\langle X\rangle = \int_{V} X(\mathbf{x})P(\mathbf{x})d\mathbf{x} \tag{5}$$

where $P(\mathbf{x})$ is the coordinate space probability

$$P(\mathbf{x}) = \frac{1}{Z}\exp\left(-\beta\mathcal{V}(\mathbf{x})\right) \tag{6}$$

In the realm of classical physics the momentum integrations can be done easily and one gets

$$Q = \frac{1}{N!}\left(\frac{2\pi m k_{\mathrm{B}}T}{h^2}\right)^{3N/2} Z \tag{7}$$

where

$$Z = \int_{V}\exp\left(-\beta\mathcal{V}(\mathbf{x})\right)d\mathbf{x} \tag{8}$$

Z is called the classical configuration integral.

2.2 Computational Methods

Before going into the details of the computational methods, some considerations are given on the type of ensembles that are manageable in MD simulations. The derivations up to now, as well as all of the following derivations apply only to the NVT-, i.e. the canonical ensemble. Thus, for the equations being applicable, the number of particles N, the volume V and the Temperature T are to held constant, which is a trivial task for N and V. Considering the temperature, there are several different *thermostats* available for MD simulations. Which thermostat to use, does not seem to be crucial. To be on the save side, however, the natural choice appears to be the Nose-Hoover thermostat[9], which, while being quite robust and stable, can be shown to provide a correct representation of the canonical ensemble. Extensions of the theory to other, such as the μVT (grand canonical) or the NPT-ensemble are not always straightforward but possible in principle; these extensions, however, will not be discussed here. For the sake of completeness it is also stressed that, for the pressure and temperature ranges of interest the difference between ΔA and ΔG is usually negligible [10].

2.2.1 The Free Energy Problem

An MD simulation provides a means for calculating any physical property that is a function of coordinates and momenta. When one solves the (classical) equations of motion in an MD simulation, one can calculate time averages of the functions of interest. As a consequence of the ergodic theorem, such a time average equals the corresponding ensemble average in equation 4. In other words, an MD-run produces a configuration of ensembles consistent with the probability density $P(\mathbf{x}, \mathbf{p})$. Since Q in equation 2 is the canonical partition function, a constant temperature MD has to be used, for all the following derivations to apply. The interesting physical property is calculated at each, or at each n-th time-step of the simulation — n depending on the correlation time of that property —

and the resulting mean value is expected to converge to the ensemble average for sufficiently long simulation times. What sufficiently means in this context, depends on the "well behavedness" of the property, as well as of the system. The internal energy, for example, is a quite non-problematic quantity in this respect, as for systems of low up to medium complexity its value will usually converge within a few dozens of picoseconds. In contrast to the internal energy, however, the calculation of the free energy is not a straightforward task. Unlike mechanical quantities (e.g. energy, pressure), which can be expressed as averages of functions of the phase space coordinates, *thermal* functions, such as the free energy or entropy, are related to the partition function and thus to the volume of the accessible phase space. To see, why this can cause problems, the free energy will be expressed in a form similar to that of equation 5.[†] The equation for the excess configurational free energy is

$$A_{ex} = -k_{\mathrm{B}}T \ln\left(\frac{Z}{V^N}\right) \tag{9}$$

The normalization factor V^{-N} establishes that A_{ex} is defined relative to an ideal gas reference state. Inserting unity in the form of

$$1 = V^{-N} \int \cdots \int \exp\left[\beta\mathcal{V}(\mathbf{x})\right] \exp\left[-\beta\mathcal{V}(\mathbf{x})\right] d\mathbf{x} \tag{10}$$

into the argument of the logarithm in equation 9 and inverting results in

$$A_{ex} = +k_{\mathrm{B}}T \ln\left[\frac{\int \cdots \int \exp\left[\beta\mathcal{V}(\mathbf{x})\right] \exp\left[-\beta\mathcal{V}(\mathbf{x})\right] d\mathbf{x}}{\int \cdots \int \exp\left[-\beta\mathcal{V}(\mathbf{x})\right] d\mathbf{x}}\right] \tag{11}$$

$$A_{ex} = kT \ln \int \cdots \int \exp\left[\beta\mathcal{V}(\mathbf{x})\right] P(\mathbf{x}) d\mathbf{x} = kT \ln\langle \exp\left[\beta\mathcal{V}(\mathbf{x})\right]\rangle \tag{12}$$

In principle equation 12 provides a means for the calculation of the excess free energy in an MD-simulation, determining an ensemble of configurations consistent

[†]There is a comprehensive review article by Beveridge and DiCapua [11] on the topic, and the next paragraph follows essentially the arguments given there.

with the probability function, $P(\mathbf{x})$, and integrating over all space as in the determination of the average energy. However, the argument of the exponential function in equation 12 is positive, thus, high energy configurations give the largest contribution to the integral. But these high energy configurations are scarcely sampled during an MC or MD simulation, which results in a *very* slow convergence of free energy calculations.

This rather intuitive argument can be derived more rigorously by expanding the exponential term of equation 12

$$\exp\left[\beta\mathcal{V}(\mathbf{x})\right] = 1 + \beta\mathcal{V}(\mathbf{x}) + \frac{1}{2!}(\beta\mathcal{V}(\mathbf{x}))^2 + \cdots \tag{13}$$

The ensemble energy average becomes

$$\langle\exp\left[\beta(\mathbf{x})\right]\rangle = 1 + \langle\beta\mathcal{V}(\mathbf{x})\rangle + \frac{1}{2!}\left\langle(\beta\mathcal{V}(\mathbf{x}))^2\right\rangle + \cdots \tag{14}$$

and the corresponding expansion for the free energy is

$$A_{ex} = k_{\mathrm{B}}T\ln\left\{1 + \langle\beta\mathcal{V}(\mathbf{x})\rangle + \frac{1}{2!}\left\langle(\beta\mathcal{V}(\mathbf{x}))^2\right\rangle + \cdots\right\}. \tag{15}$$

Thus, one can clearly see that for the evaluation of the free energy it is necessary to not only calculate the ensemble average of the configurational energy, but also of higher powers to an extent dependent on the radius of convergence of the expansion. It is a well known fact that fluctuations converge slower than mean values; a problem one encounters, for example, when trying to calculate heat capacities.

A way out of this dilemma appears when one recalls that free energy differences, rather than absolute free energies, are the quantities of interest. We are interested in the free energy difference ΔA between two well defined states, here denoted i and f (initial and final), characterized by different configurational partition functions Z_i and Z_f, that is implicitly by two potential energy functions, U_i and U_f. In a manner similar to what we did for the absolute free energy, we

can write the free energy difference between state i and f as [12]

$$\Delta A = A_f - A_i = -k_{\mathrm{B}}T \ln\left(\frac{Z_f}{Z_i}\right) \tag{16}$$

$$= -k_{\mathrm{B}}T \ln \frac{\int\limits_V \exp\left(-\beta U_f(\mathbf{x})\right) d\mathbf{x}}{\int\limits_V \exp\left(-\beta U_i(\mathbf{x})\right) d\mathbf{x}} \tag{17}$$

We insert unity in the form

$$1 = \exp\left(-\beta U_i(\mathbf{x})\right) \exp\left(\beta U_i(\mathbf{x})\right) \tag{18}$$

into equation 17 to get

$$\Delta A = -k_{\mathrm{B}}T \ln \frac{\int\limits_V \exp\left(-\beta U_f(\mathbf{x})\right) \exp\left(-\beta U_i(\mathbf{x})\right) \exp\left(\beta U_i(\mathbf{x})\right) d\mathbf{x}}{\int\limits_V \exp\left(-\beta U_i(\mathbf{x})\right) d\mathbf{x}} \tag{19}$$

$$= -k_{\mathrm{B}}T \ln \int\limits_V \exp\left(-\beta(U_f(\mathbf{x}) - U_i(\mathbf{x}))\right) P_i(\mathbf{x}) d\mathbf{x} \tag{20}$$

$$= -k_{\mathrm{B}}T \ln \langle \exp\left(-\beta \Delta U(\mathbf{x})\right) \rangle_i \tag{21}$$

The usage of equation 21 for free energy calculations is called perturbation method (PM) or exponential formula (EF). It will be discussed briefly in section 2.2.3. The present work, however, will primarily remain confined to *thermodynamic integration* (TI), which is another method commonly used in this area. TI also exploits the fact that differences are easier to calculate than absolute free energies.

2.2.2 Thermodynamic Integration

Thermal quantities, such as the Helmholtz or the Gibbs energy are functions of the partition function Q, while mechanical quantities are functions of a first derivative of the partition function with respect to another thermodynamic quantity. Internal energy and pressure, for example, are given as,

$$U = k_{\mathrm{B}}T^2 \left(\frac{\partial \ln Q}{\partial T}\right), \qquad P = k_{\mathrm{B}}T \left(\frac{\partial \ln Q}{\partial V}\right) \tag{22}$$

The fact that these quantities are relatively easy to determine by MD simulations.[‡] suggests that the derivative of A with respect to any variable may behave better than A itself.

A prerequisite for TI is the so called *coupling parameter approach* [13]. It is always possible to define the internal energy U as a function of a parameter λ (the coupling parameter), such that $\mathrm{U}(\lambda = 0) = \mathrm{U}_i$ and $\mathrm{U}(\lambda = 1) = \mathrm{U}_f$, thereby defining a *thermodynamic* path from U_i to U_f. The simplest way of defining such a function is

$$U(\mathbf{x}, \lambda) = (1 - \lambda)U_i(\mathbf{x}) + \lambda U_f(\mathbf{x}) \tag{23}$$

The internal energy — just as the free energy — is a state function, that is, the difference depends only on the position of the end points of a transition and not on the transition path itself. As long as it is continuous, this path can thus be non-physical, i.e., not feasible in a *real world* experiment. Given an $\mathrm{U}(\lambda)$ and, thereby, implicitly — via equation 9 — an $\mathrm{A}(\lambda)$, the free energy difference $\Delta\mathrm{A}$ between the two states A_i and A_f can be formally written as [14]

$$\Delta A = \int_0^1 \frac{\partial A(\lambda)}{\partial \lambda} d\lambda \tag{24}$$

In contrast to the absolute free energy, this difference can be conveniently expressed as an ensemble average. When writing the free energy

$$A(\lambda) = -k_{\mathrm{B}} T \ln Z(\lambda) \tag{25}$$

and the configurational partition function

$$Z(\lambda) = \int_V \exp[-\beta U(\mathbf{x}, \lambda)] d\mathbf{x} \tag{26}$$

as functions of λ, their derivatives with respect to λ are

$$\frac{\partial A(\lambda)}{\partial \lambda} = -k_{\mathrm{B}} T \left(\frac{\partial \ln Z(\lambda)}{\partial \lambda} \right) = -\frac{k_{\mathrm{B}} T}{Z(\lambda)} \frac{\partial Z(\lambda)}{\partial \lambda} \tag{27}$$

[‡]Well, at least the internal energy, calculation of the pressure involves peculiar problems in its own right.

$$\frac{\partial Z(\lambda)}{\partial \lambda} = -\beta \int_V \frac{\partial U(\mathbf{x},\lambda)}{\partial \lambda} \exp[-\beta U(\mathbf{x},\lambda)] d\mathbf{x} \tag{28}$$

Substituting (28) into (27) results in

$$\frac{\partial A(\lambda)}{\partial \lambda} = \frac{1}{Z(\lambda)} \int_V \frac{\partial U(\mathbf{x},\lambda)}{\partial \lambda} \exp[-\beta U(\mathbf{x},\lambda)] d\mathbf{x} \tag{29}$$

or

$$\frac{\partial A(\lambda)}{\partial \lambda} = \left\langle \frac{\partial U(\mathbf{x},\lambda)}{\partial \lambda} \right\rangle_\lambda \tag{30}$$

where the subscript $_\lambda$ indicates that the phase space density is a function of λ, i.e.,

$$P(\mathbf{x},\lambda) = \frac{\exp[-\beta U(\mathbf{x},\lambda)]}{\int_V \exp[-\beta U(\mathbf{x},\lambda)] d\mathbf{x}} \tag{31}$$

is the probability of finding the system in configuration $\mathbf{x}$ at a position λ between the initial and final state of the transformation. Finally,

$$\Delta A = \int_0^1 \left\langle \frac{\partial U(\mathbf{x},\lambda)}{\partial \lambda} \right\rangle_\lambda d\lambda \tag{32}$$

Equation 32 is the key-equation of thermodynamic integration. One calculates $\langle \partial U(\mathbf{x},\lambda)/\partial\lambda \rangle_\lambda$ for several λ-values between 0 and 1, and ΔA is obtained by numerical integration, using for example the trapezoidal rule. When the hybrid potential is linear in λ, i.e., if it has the form given in equation 23, then

$$\left\langle \frac{\partial U}{\partial \lambda} \right\rangle_\lambda = \Delta U = U_f - U_i \tag{33}$$

is calculated for n λ-values (windows), and equation 32 takes the form

$$\Delta A = \Delta\lambda \sum_{i=1}^{n} \langle \Delta U \rangle_{\lambda_i} \tag{34}$$

In practice there are two different ways how one can perform TI. The method presented in the last paragraph is called *windowing* (WI). Depending on the actual system and the belief of the involved scientist, the number of simulations

at distinct λ-values can vary from 5 up to a few hundred. Consequently, the spacing $\Delta\lambda$ and the number of time steps used for one window (should) vary accordingly. The extreme case of one distinct value of λ corresponding to each time-step of the MD is called *slow growth* (SG). The latter method, while minimizing the error made by numerical integration, has been criticized for providing non-equilibrium conditions throughout the whole MD-run and, thereby, not meeting the requirements of the angular brackets in equation 32 [15]. Numerous papers on the (dis)advantages of different window-sizes, simulation lengths per window, over-all simulation length etc. have been published, and the reader is referred to Refs [15, 16, 17, 18, 19] and the references there for more details about the optimization of TI calculations.

2.2.3 Other Methods

Other methods for the determination of free energies by computer simulation are available, and will be described very briefly in this section. In the context of MD, the most frequently used methods besides TI are the already mentioned *perturbation method* (PM) and *potential of mean force* (PMF) calculations.

Equation 21 is the foundation of for the perturbation method. For clarity, it is given once again.

$$\Delta A = -k_{\mathrm{B}}T \ln \langle \exp[-\beta \Delta U(\mathbf{x})] \rangle_{\lambda=0} \tag{35}$$

Using this equation, one can, in principle, calculate a free energy difference in a single simulation run. However, the two systems represented by U_i and U_f must not be too different, i.e., the two partition functions have to overlap within a considerable range of the phase space — so that the difference can be regarded as a small perturbation — that is where the name of this method comes from. In practice, the path for a given transition is divided into several steps of convenient size and PM-calculations are performed as a series of a separate simulations. The accuracy of the results and the computational efficiency of PM are comparable to

those of TI. There may, however, be some systems and corresponding free energy differences that can be treated better by one of the two methods although there seem to exist no general guidelines for this kind of decision.

For the special case of two of the N particles of a system fixed in space at a distance R, the expression of the free energy takes the form

$$A(R) = -k_{\mathrm{B}}T \ln[g(R)] + constant \tag{36}$$

Here $g(r)$ is the radial distribution function,

$$g(r) = \frac{N(N-1)}{\rho} \exp\left(-\beta U(\mathbf{x}^N|R)\right) d\mathbf{x}^{N-2} \tag{37}$$

where $(\mathbf{x}^N|R)$ denotes a configuration of N particles, subject to the condition that two of them are fixed at a distace R. A(R) is the reversible work involved in the association of the two particles from infinite separation to the distance R, in solution. The derivative of A(R) with respect to R is the force acting between the two particles, including both direct and solvent averaged contributions. Therefore, A(R) is called the potential of mean force, often denoted as w(r). R can represent not only the distance between two particles, but an arbitrary degree of freedom, such as a torsional angle or a generalized structural transition of the system. The calculation of $g(R)$ suffers from the same sampling problems as discussed above for the free energy.

For both, PMF and PM calculations, a solution for this problem can be a special kind of importance sampling, accomplished by modifying the Hamiltonian of the system in an appropriate manner, so that the system visits the desired portion of phase space more frequently [20]. Since the Hamiltonian is modified, a free energy difference cannot be obtained by evaluating the resulting set of configurations directly. It is possible, however, to obtain meaningful results by applying a kind of backward transformation to the calculated configurations. In the context of MC simulations this technique is called umbrella sampling and numerous variations of this method, as well as extensions to use it in MD, have been proposed [21, 22].

For a more elaborate account of these methods the reader is once again referred to some review articles [11, 23] and references there.

2.2.4 Some Practical Aspects

Up to this point the dicussion has been rather abstract. Now the question is adressed which types of free energy differences and transitions are manageable with MD as the method of choice. The range of applications considered here will remain confined to the investigation of biomolecular systems. We stress once more, that by computer-simulation — just as in *real world* experiments — only free energy differences as opposed to absolute free energies can be calculated. Transitions can, in principle, be carried out by changing arbitrary parameters of the potential energy function. Equation 38 shows the typical potential energy function of an all-atom MD-force-field.

$$U = \sum_{i<j}^{N_s} 4\epsilon_{ij} \left\{ \left(\frac{\sigma_{ij}}{r_{ij}}\right)^{12} - \left(\frac{\sigma_{ij}}{r_{ij}}\right)^{6} \right\} + \sum_{i<j}^{N_s} \frac{q_i q_j}{r_{ij}} + \sum_{i=1}^{N_b} k_i^b (b_i - b_{i,eq})^2 + \sum_{i=1}^{N_a} k_i^a (\alpha_i - \alpha_{i,eq})^2 + \sum_{i=1}^{N_d} k_i^d [1 + cos(n_i \theta_i - \gamma_i)] \quad (38)$$

with N_s, N_b, N_a and N_d being the number of atomic sites, bonds, angles and dihedral angles, respectively. Parameters, such as partial charges q_i or equilibrium bond lengths $b_{i,eq}$, have to be provided for the bonded and non-bonded interactions of a number of types of atomic sites, and their combinations. U_i and U_f as introduced by equation 23 are uniquely defined by a set of these parameters. The initial and final potentials represent two completely or partially different ensembles of molecules. In practice, only certain types of free energy differences can be calculated by MD. Fortunately, these types are frequently complementing the data obtained by laboratory experiments. Let us consider a simple example to clarify what the restrictions are.

Assume that we are interested in the free energy of solvation of two different molecules, called X and Y. Our first condition is fulfilled, since we are talking

about a free energy *difference* ΔA, actually the difference of two differences $\Delta\Delta$A, i.e., the difference of the differences between the free energies of the molecules in, for example, aqueous solution and in some reference states (usually the ideal gas state). Just as in the *real world* experiment, we now have to consider the path connecting these states. Experimentally, one can measure the free energy of transferring a molecule from the gas phase into aqueous solution. The over-all simulation time of MD is, however, of the order of 1 ns and the practicable sample-size rarely exceeds 100,000 particles, i.e., we can only simulate small changes (transitions) over a short time-scale. Consequently, we cannot put our molecules into the gas-phase above a liquid sample of water and wait until they diffuse into the solvent. Further, as will become clearer in the following section, the direct insertion of the molecule into a water sample is — at least for big molecules — still a difficult task. An intriguing solution to our problem appears when we are ready to extend our imagination concerning the transition path between two thermodynamic states. Therefore, we take a look at figure 1, a thermodynamic cycle and a concept of crucial importance for most free energy calculations. The states connected by the thermodynamic cycle in figure 1 are X_{gas} and Y_{gas}, each of the two molecules in the ideal gas phase, as well as X_{solv} and Y_{solv}, each of the two molecules in aqueous solution. The transition paths denoted by ΔA_1 and ΔA_2 represent the free energies of solvation. ΔA_3 and ΔA_4 represent so called *alchemical* transitions, i.e., transitions involving the direct metamorphosis of one type of molecule into another. Provided the two types of molecules are not too different in shape and size, such a modification involves only minor changes of the potential energy function in the course of an MD simulation. Thus, for this kind of transition the condition concerning time and size scale is met, and the transition is pefectly manageable by computer simulation. Since, on the other hand, the free energy is a state function, we have $\sum_{i=1}^{4} \Delta A_i = 0$ or $\Delta\Delta A = \Delta A_1 + \Delta A_2 = -\Delta A_3 - \Delta A_4$. So we do not have to calculate ΔA_1 or ΔA_2 at all to get $\Delta\Delta$A. As a matter of fact, quite a few types of free energy differences can be

calculated with MD, when the corresponding transition path is properly divided into manageable segments of a thermodynamic cycle. In order to concretize the

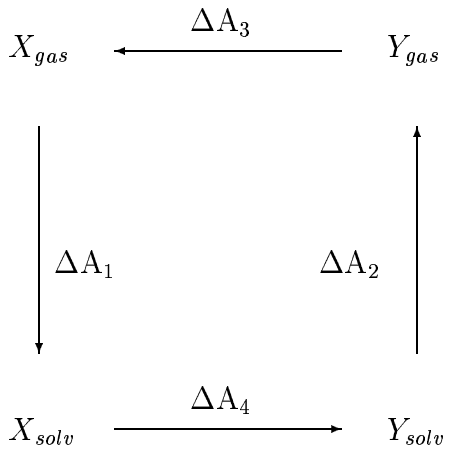

Figure 1: Thermodynamic cycle

idea, two more examples for the usefulness of a thermodynamic cycle as tool for the interpretation of free energy data are given.

Receptor-ligand interactions, the relative stability of complexes with different ligands and the mechanisms of recognition and binding are frequently encountered issues in biochemistry. Figure 2.2.4 shows the corresponding thermodynamic cycle. L1 and L2 are two different ligands and R-L1 and R-L2 the respective receptor-ligand complexes. In each of the four connected states the components are in aqueous solution. Just as in the prceeding example, the transition-paths used in a laboratory experiment, i.e., ΔA_1 and ΔA_2 are not manageable by MD — too extensive changes are involved and the sampling problem would be formidable. ΔA_3 and ΔA_4 on the other hand involve only small changes, provided the two ligands are sufficiently similar. The quantity $\Delta\Delta A = \Delta A_1 + \Delta A_2 = -\Delta A_3 - \Delta A_4$ can be used to compare — at least qualitatively — the binding affinities of the two ligands. Another interesting biochemical application is the

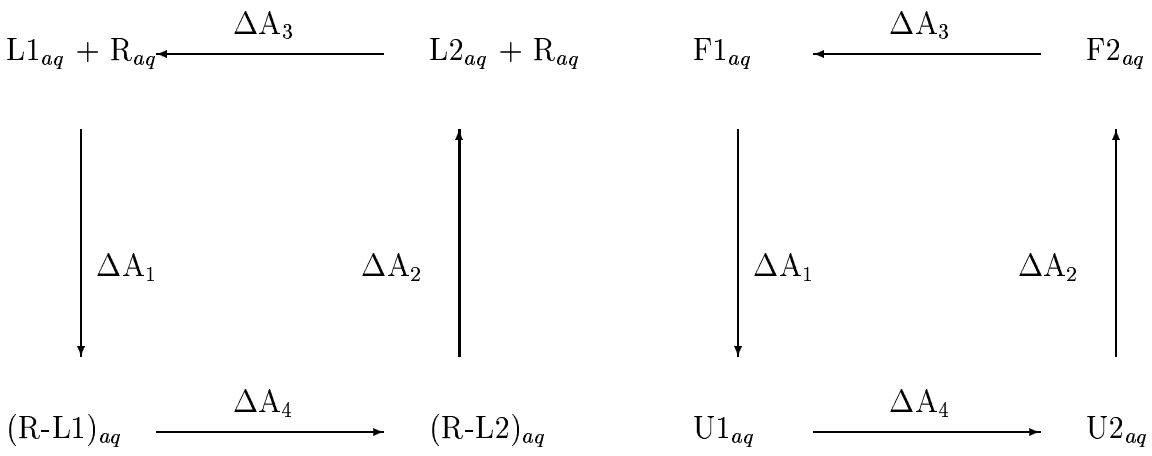

Figure 2: More thermodynamic cycles

calculation of the effects of point-mutations on the stability of a protein in solution. An appropriate thermodynamic cycle is drawn in figure 2. $U1_{aq}$ and $U2_{aq}$ are two unfolded versions of a protein differing only in one amino acid. $F1_{aq}$ and $F2_{aq}$ are the folded equivalents. For the same reasons as stated above ΔA_1 and ΔA_2 cannot be calculated by MD. As opposed to the folding of the entire protein, the mutation of a single amino acid, however, is computationally feasible. Thus ΔA_3 and ΔA_4 can be calculated by simulation and the sign and the magnitude of $\Delta\Delta A = \Delta A_1 + \Delta A_2 = -\Delta A_3 - \Delta A_4$ will allow the estimation of the relative stabilities of the two variants.

For more examples of the application of thermodynamic cycles in the given context see Ref [23] and references there. As a matter of fact, ΔA_1 and ΔA_2 in figure 1 can also be calculated directly by inserting a particle into (or removing it from) a box of solvent, i.e., by switching the non-bonded interactions from zero to the appropriate value (or *vice versa*). At least for small molecules this is possible. Going this path, however, is a source of peculiar problems and requires special precautions, which will be discussed in the next section.

2.2.5 The Origin Singularity Arising in Particle Insertion

As indicated above, one can calculate free energy differences for every sort of transition that can be mimicked by changing any combination of the force field parameters. The non-bonded interactions of one particle/molecule with the rest of the system can be switched off (on) completely, in order to calculate the free energy of solvation of this particle/molecule. A certain residue within a large molecule can be replaced by a substitute of considerably different shape and size, e.g. the replacement of a small amino acid within a peptide by a larger one, as, for example, the transition Ala $\rightarrow$ Tyr. Especially when performed in solution, attempts to calculate free energy differences of this type can encounter severe problems, unless special simulation techniques are employed. The technical term for these problems is *Van der Waal's endpoint problem (or catastrophe)* (VdWEP) and comprises two issues:

1) Consider a particle situated in a box of solvent molecules. Let U_i ($U(\lambda = 0)$) be the Hamiltonian with the particle entirely present and U_f ($U(\lambda = 1)$) the Hamiltonian with all the interactions between the particle and the rest of the system set to zero. Now change λ in a stepwise fashion from 0 to 1 during an MD simulation. At $\lambda = 1$ the particle has technically vanished, i.e., the other particles will not see it anymore. However, $\langle \partial U/\partial \lambda \rangle_1$, i.e., $\langle U_f - U_i \rangle_1$ in the linear case, has to be calculated. Because of the lack of interactions, the solvent molecules can get arbitrarily close to the "vanished" particle. This leads to *huge* numbers for the potentials and their derivatives and eventually to divisions by zero for overlap configurations.

2) The second problem is not as intuitively understandable as the first one, and for an exact derivation of the underlying mathematics the reader is referred to a paper by Simonson [19]. For potentials of the form

$$U(r) = \lambda^{\alpha} A r^{-n} \tag{39}$$

i.e., the interactions of the accordant particle are entirely switched off at one

end-point ($\lambda = 0$) of the transition path, he could show that

$$\langle \partial U(\lambda)/\partial\lambda \rangle \propto \lambda^{3\alpha/n-1}, \lambda \to 0 \tag{40}$$

$\langle \partial U/\partial\lambda \rangle$ diverges for $\lambda \to 0$, if $\alpha = 1$, i.e., U is a linear function of λ. Although the free energy difference, the integral $\int_0^1 \langle \partial U(\lambda)/\partial\lambda \rangle \, d\lambda$, is finite, attempts to calculate the diverging integrand in the MD simulation lead to very large fluctuations and, consequently, to extremely slow convergence of ΔA for λ approaching 0.

There are basically three different ways, one can try to bypass the VdWEP:

Extrapolation: For $\alpha = 1$ and $n = 12$, i.e. the repulsive part of a linearily scaled LJ-potential equation 40 becomes

$$\langle \partial U(\lambda)/\partial\lambda \rangle \propto \lambda^{-\frac{3}{4}}, \lambda \to 0 \tag{41}$$

For the complete Lennard-Jones potential this equation is still valid since only the repulsive part of the potential determines the shape of the free energy at the origin. Using this formula, one can extrapolate $\langle \partial U(\lambda)/\partial\lambda \rangle$ for $\lambda \to 0$, thus avoiding the necessity to calculate $\langle \partial U(\lambda)/\partial\lambda \rangle_{\lambda=0}$. One proceeds as follows: $\langle \partial U(\lambda)/\partial\lambda \rangle_\lambda$ is calculated up to a value λ_s near zero in the usual manner, followed by simulations for a series of λ-values between λ_s and zero. The parameters a and b of a function

$$y = a + bx^{-3/4} \tag{42}$$

are evaluated by fitting the calculated values of the derivative to this function. The resulting function is integrated to yield ΔA for $0 \leq \lambda \leq \lambda_s$.

The advantage of this method is its simplicity and ease of combination with existing methods, i.e., it does not require any new computer code. The drawback of the method is twofold: Not only has $\langle \partial U(\lambda)/\partial\lambda \rangle$ to be calculated for additional windows between λ_s and 0, but usually the time-step for the simulations at these λ-values has to be reduced considerably; otherwise the movement

of a vanishing particle within a single time step could lead to immense forces, resulting in numerical instabilities. Second, Equation 41 is valid only for soft-core or Lennard-Jones-like potentials. If a coulomb potential is involved, the partial charges need to be turned off first in a separate simulation. Further, the estimation of the error introduced due the extrapolation is quite difficult.

Nonlinear λ-Scaling: The form of equation 40 suggests another way of coping with the VdWEP: for $\alpha \geq 4$ the λ-derivative of the potential will not diverge anymore. Methods based on this fact are widely used in the context of free energy simulations. A related method — scaling not the total potential, but the LJ-parameters σ — can be shown to be essentially equivalent to scaling the total potential with λ^{12} in the LJ-case. However, just like the extrapolation-method presented in the preceding paragraph, non-linear λ-scaling is unable to cope with all the problems due to the VdWEP. In contrast to MC, the accurate calculation of the potential is not sufficient to get reliable results using MD. In addition to the potential, its first derivatives with respect to the coordinates, i.e., the forces, also have to be calculated. If these forces change very fast, which can definitely happen at λ close to 0, despite non-linear λ-scaling, it becomes increasingly intricate to maintain the desired precision in the integration of the equations of motion, and, again, the time-step has to be reduced, resulting in a loss in efficiency of the simulation.

Separation Shifted Potentials: In 1994 two papers [3, 4], introduced a new method to circumvent the VdWEP. The name of the method: *separation shifted scaling* (SSS) can be taken quite literally. The Lennard-Jones-potential is modi-

fied as follows

$$
\begin{aligned}
U_{LJ}(r,\lambda) &= (1-\lambda)U^i_{LJ}(r,\lambda) + \lambda U^f_{LJ}(r,\lambda) \\
U^i_{LJ}(r_{ab},\lambda) &= 4\epsilon^i_{ab}\left(\frac{{\sigma^i_{ab}}^{12}}{(r^2+\delta_v\lambda)^6}\frac{{\sigma^i_{ab}}^{12}}{(r^2+\delta_v\lambda)^3}\right) \\
U^f_{LJ}(r_{ab},\lambda) &= 4\epsilon^f_{ab}\left(\frac{{\sigma^f_{ab}}^{12}}{(r^2+\delta_v(1-\lambda))^6}\frac{{\sigma^f_{ab}}^{12}}{(r^2+\delta_v(1-\lambda))^3}\right)
\end{aligned}
\tag{43}
$$

In addition to the total potential the distance between the mutated particle and the other particles is scaled when using SSS. This distance is augmented by the term $\sqrt{\delta_v\lambda}$ for U_i and $\sqrt{\delta_v(1-\lambda)}$ for U_f, resulting in the potential and its derivatives with respect to the coordinates and λ being finite for all particle distances including $r = 0$. The extent of scaling is determined by the parameter δ_v. For the equations for the free energy being valid, δ_v can be set to an arbitrary value. However, to ensure numerical stability and precision of the results, a convenient value for δ_v has to be determined by trial and error. The computational effort for such calculations is negligible. As a consequence of this convenient modification of the potentials, both of the above-mentioned problems, arising for particle insertion or annihilation vanish. Separation shifted LJ-potentials and forces for various values of δ_v are depicted in figures 3 and 4. For the states $\lambda = 0$ and $\lambda = 1$, the original Lennard-Jones-potential is restored, i.e., only the path between the two states differs from the case of linear λ-scaling, whereas the endpoints of the transition and, therefore, the free energy difference are not affected by the separation shifted scaling since the free energy is path-independent.

Since the LJ-potential usually dominates the interaction at small distances by far, it was at first assumed that SSS has to be applied only for the LJ-potential. It turned out, however, that, in addition to the LJ-potential also the Coulomb potential has to be scaled in a similar manner. In figure 5 the sum of the Coulomb and the LJ forces for a single pair of sites bearing LJ-centers as well as partial

Figure 3: Separation shifted potentials, Lennard-Jones energy for $\lambda = 0.5$ and different parameters δ_v, on two scales

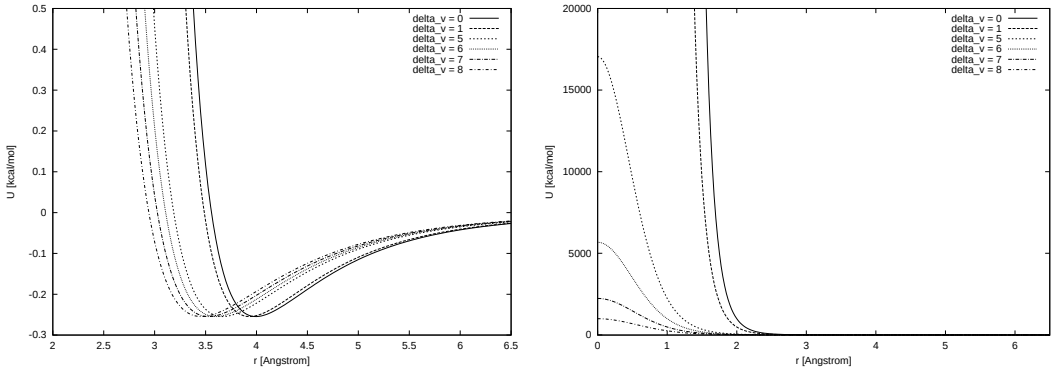

Figure 4: Separation shifted potentials, Lennard-Jones forces for $\lambda = 0.5$ and different parameters δ_v, on two scales

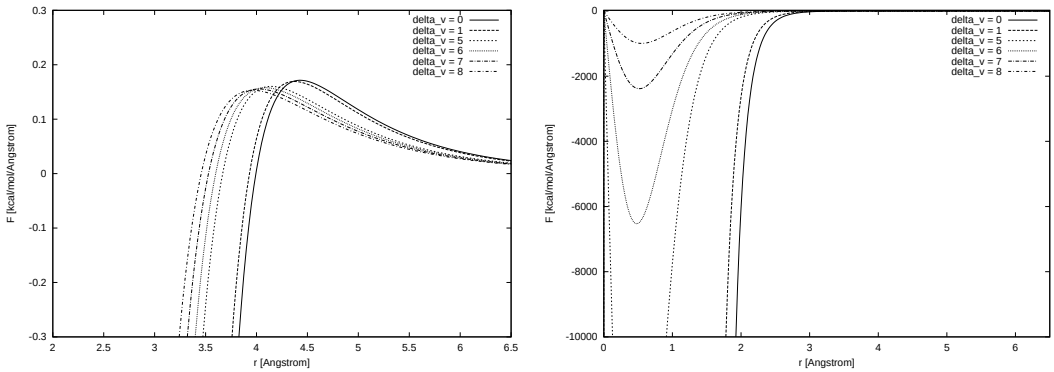

Figure 5: The sum of the LJ and the coulomb forces for different parameters δ_v, see text for details

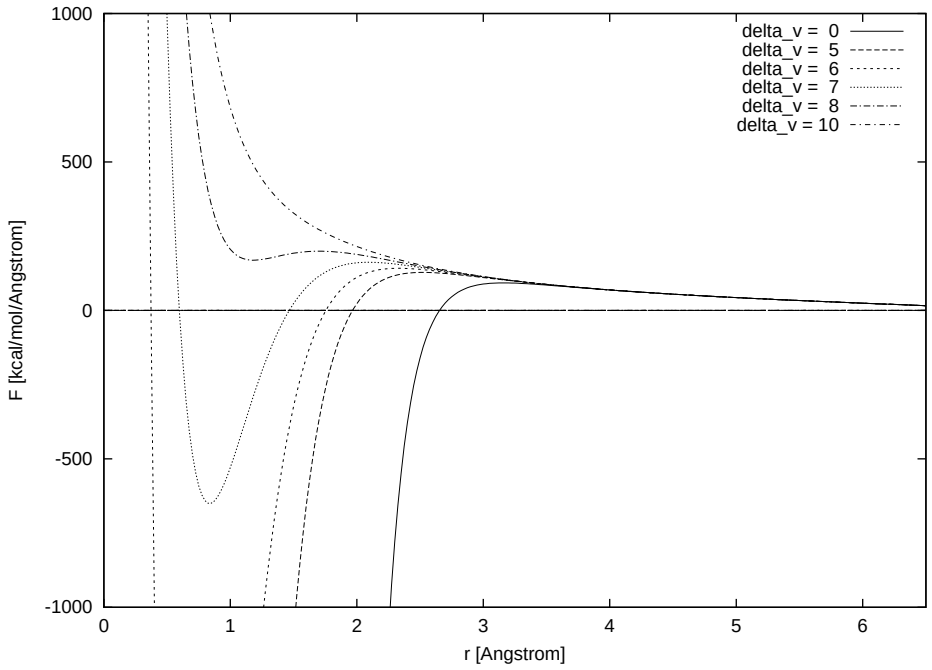

charges is drawn as a function of distance for various δ_v's.[§] Apparently the coulomb-forces dominate the interaction at small distances for $\delta_v > 8$ Å^2. For two particles with different sign, this could lead to a "nuclear melt-down", i.e., the two particles overlap entirely, followed by a break down of the program due to floating point overflows and devisions by zero. Since for values of δ_v much lower than 5 Å^2 the VdWEP is partially restored, the usage of a separation shifted Coulomb potential seems to be the appropriate solution. The Coulomb potential

[§]The relevant non-bonded parameters were set to $r_{min,i} = 1.0$, $\epsilon_i = -0.30$, $r_{min,f}/2 = 2.0$, $\epsilon_f = -0.50$, $q_i = \pm 1$ and $q_f = \pm 2$ respectively.

gets modified in a similar way as the LJ-potential to become

$$\begin{aligned} U_{el}(r,\lambda) &= (1-\lambda)U_i(r,\lambda) + \lambda U_f(r,\lambda) \\ U_i(r_{ab},\lambda) &= q_i^b q_i^b \left(r_{ab}^2 + \delta_e \lambda\right)^{\frac{1}{2}} \\ U_f(r_{ab},\lambda) &= q_f^a q_f^a \left(r_{ab}^2 + \delta_e (1-\lambda)\right)^{\frac{1}{2}} \end{aligned} \tag{44}$$

2.2.6 Treatment of Long range Interactions

The usual topological setup for a MD-simulation of a liquid or a solvated system is to confine the molecules to a cubic box. In order to avoid surface effects one employs toroidal or periodic boundary conditions (TBC, PBC) together with the so called minimum image convention. Although state of the art computers are able to cope with simulations of up to millions of particles the suppression of surface effects by just enlarging the system will remain unrealistic for quite a long time to come.

When using TBC the interaction of a molecule with its own image in a neighbouring box can lead to severe artifacts and, therefore, only the interactions of pairs of particles within a certain cutoff (smaller than half the length of the cubic box) are permitted.[¶] The neglect of all the interactions beyond this cutoff is justified only for molecules that are uncharged and have no permanent dipole moment since the remaining Van der Waals (VdW) interactions are short ranged. Electrostatic charge-charge and dipole-dipole interactions are long ranged, i.e. they are described by a potential $Ur_{ij} \propto r_{ij}^{-1}$ or $Ur_{ij} \propto r_{ij}^{-3}$, respectively. Neglecting these interactions beyond the cutoff leads to artifacts and wrong results for many physical quantities [24]. If and for what types of systems free energy differences are among these quantities is subject of ongoing debate; some pertinent results will be reported in chapter 5.2. This section briefly describes the different methods that are commonly used to account for or at least mitigate the effects of the

[¶]This restriction does not apply to the ewald method.

truncation of long range interactions.

Tapering functions: An immediately obvious effect of a straightforward truncation of long range interactions in the course of an MD simulation is the lack in energy conservation due to the discontinuity of the potential function at the cutoff distance. This problem can be solved by employing so called tapering functions, i.e., by changing the functional form of the Coulomb-potential so that it smoothly vanishes when the particle distance approaches the cutoff radius. In figures 6 to 9 the Coulomb potential as well as its smoothened version for a dimer of charged particles as a function of distance are depictured for several different types of tapering functions. There are essentially two main-types of tapering functions available:

- *SWITCHING:* In addition to the actual cutoff radius r_c, a second distance, the inner cutoff r_i ($0 < r_i < r_c$) is defined. For $r_i < r < r_c$ the potential U(r) is multiplied with a switching function SW(r), the actual functional form of which can differ. Its essential features are: $\mathrm{SW}(r_c) = 0$, $\mathrm{SW}(r_i) = 1$ and between r_i and r_c SW(r) decays monotonically and continuously changing the potential smoothly from the unmodified value at r_i to zero at r_c.

- *SHIFTING:* The potential function U(r) is shifted over the whole range between $r = 0$ and $r = r_c$, either by just adding the constant offset $-U(r_c)$, or by multiplying with a shifting function SH(r). A shifting function can be considered as the extreme case of a switching function with $r_i = 0$.

Together with the potential its derivative, i.e., the force is to be modified accordingly. It is, of course, possible to go the other way round, i.e., the forces can be *shifted* or *switched* and the accordant potential would be the integrated shifted or switched force. In this case the resulting potentials not necessarily vanish at the cutoff distance. This is, however, no problem since the potential can be modified

Figure 6: Tapering functions: shifted potential, $r_i = 6.5, r_c = 7.5$

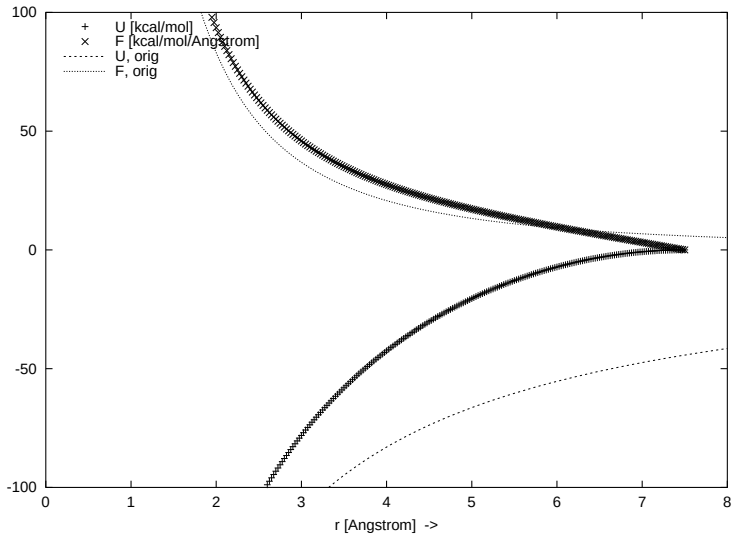

Figure 7: Tapering functions: switched potential, $r_i = 6.5, r_c = 7.5$

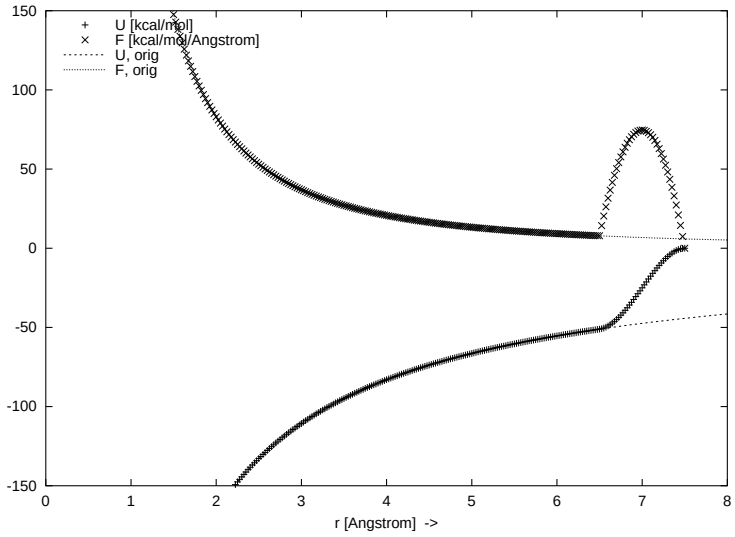

Figure 8: Tapering functions: switched force, $r_i = 6.5, r_c = 7.5$

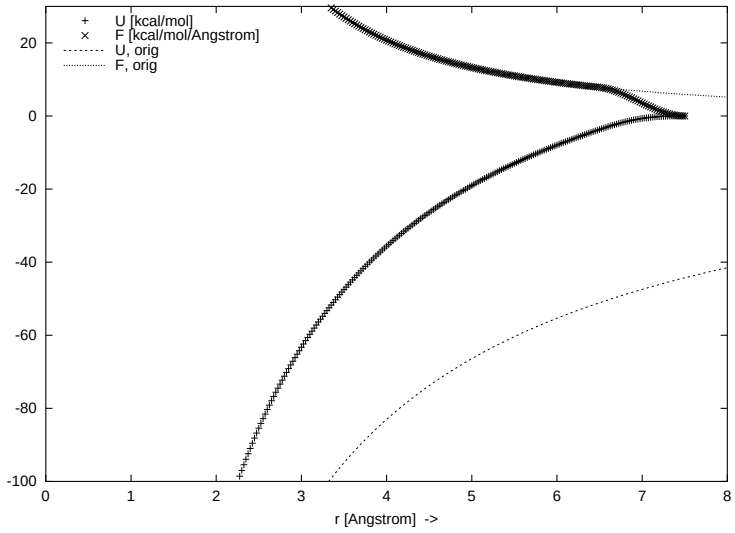

Figure 9: Tapering functions: shifted force, $r_i = 6.5, r_c = 7.5$

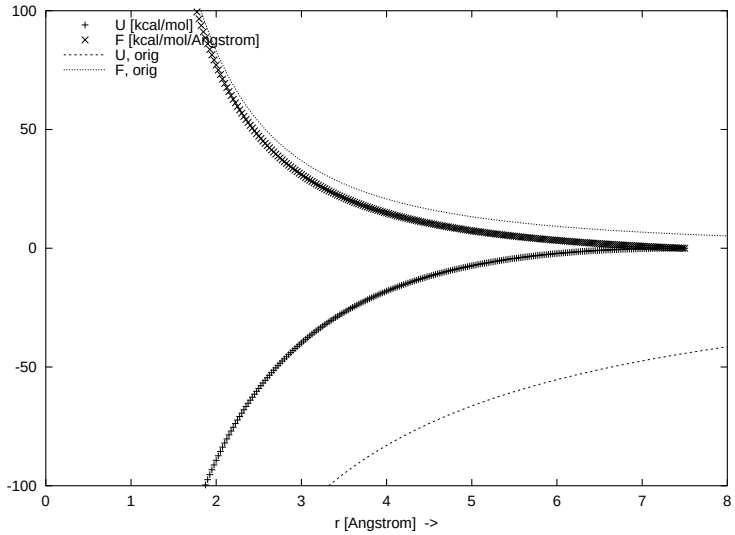

Table 1: Abbreviations for some methods of potential smoothing (tapering functions) implemented in CHARMM; For details see chapter 2.2.6

	group based cutoff	atom based cutoff
potential switching	GSW	ASWI
potential shifting		ASHF
force switching	GFSW	AFSW
force shifting		AFSH
generalized reaction field		GRF

by adding a constant, which, in turn, will not affect the forces since the derivative of a constant becomes zero anyway [24].

When one studies molecules instead of atoms in an MD-simulation, these molecules are frequently divided into groups, each consisting of several atoms. A group can consist of a single molecule, such as the TIP3P water model, or a part of a larger molecule, such as an amino acid residue of a protein.

When applying a switching or shifting function to the potential or forces in such cases, there is one additional choice: the distance r in the potential U(r) and, e.g., the switching function SW(r), can be the same for both functions. Alternatively the distance entering SW(r) can be taken to be the same for all members of a pair of groups. Usually, the distance between the centers of mass or centers of geometry of two groups is used in this case. In the first case, a particular atom can occasionally "see" only a part of a distant group when only a fraction of its "members" are within the cutoff-range (*atom based cutoff*). In the latter case only entire groups see each other (group based cutoff). This distinction may seem to be merely accidental at the first glance. It can, however turn out to be crucial under certain conditions, as will be seen in chapter 5.2.

Various forms of tapering functions have been proposed over the years, quite a few of which are implemented in CHARMM. For their functional forms, see appendix A and Ref. [25]. In Table 1 abbreviations for all the tapering functions used here are given.

Reaction Field: In the reaction field method it is assumed that any given molecule is surrounded by a spherical cavity of finite radius within which the electrostatic interactions are calculated explicitly [26]. Outside the cavity the system is treated as a dielectric continuum. The occurrence of any net dipole within the cavity induces a polarization in the dielectric, which in turn interacts with the given molecule. The model allows the replacement of the infinite Coulomb sum by a finite sum plus the reaction field. The effective pair potential in cgs-units is given by

$$u(r_{ij}) = q_i q_j \left(\frac{1}{r_{ij}} + \frac{(\epsilon_{RF} - 1)}{(2\epsilon_{RF} + 1)} \frac{r_{ij}^2}{r_c^3} \right) \tag{45}$$

with r_c the radius of the cavity and ϵ_{RF} the dielectric constant outside the cavity. This expression unfortunately leads to large fluctuations in the system Coulombic energy, due to the large step in the function at the cavity boundary, and, therefore, usually the reaction field potential is smoothened by a tapering function.

Hummer et al. introduced an extended version [6] of this concept, a *generalized reaction field* with a coulomb potential of the form

$$\phi(r_{ij}) = \frac{q_i q_j}{r_{ij}} \left(1 - \frac{r_{ij}}{r_c} \right)^4 \left(1 + \frac{r_{ij}}{5r_c} + \frac{2r_{ij}^2}{5r_c^2} \right) \tag{46}$$

$\phi(r)$ and all its derivatives are monotonic and of alternating sign, just like $\frac{1}{r}$, and $\phi(r)$ and its derivatives up to third order vanish at the cutoff r_c. This screened Coulomb interaction model yields results for test systems that agree very well with Ewald summation data.[6]

Ewald Summation Ewald summation (EW) [24], and its variations [27], are in fact the only methods, that — in a certain way — include all long range

interactions. The concept of PBC is thereby taken literally by assuming the system to be composed of an infinite number of periodic boxes. The particles in the central box interact not only with other particles in that very box, but additionally with all the periodic replicas in the surrounding infinite number of boxes. Written in cgs-units, the electrostatic energy is given as

$$U = \sum_{\mathbf{n}} \left(\sum_{i<j} q_i q_j |\vec{r}_{ij} + \mathbf{n}|^{-1} \right) \tag{47}$$

The sum over $\mathbf{n}$ is the sum over all simple cubic lattice points, $\mathbf{n} = n_x L + n_y L + n_z L$, n_x, n_y, n_z being integer and L the side length of the cubic box. In order to manage this summation, the coulomb potential for each pair of particles is written as a sum of two terms

$$u = \frac{q_i q_j}{r_{ij}} = \frac{q_i q_j}{r_{ij}} \mathrm{erfc}(\kappa r_{ij}) + \frac{q_i q_j}{r_{ij}} \mathrm{erf}(\kappa r_{ij}) \tag{48}$$

The result of this decomposition is shown in figure 10: the complementary error function renders the first term of the sum short ranged, leaving the long range contribution of the coulomb potential essentially to the second term. The relative weight of the two terms is controlled by the parameter κ. The nasty long range behavior of the second term can be coped with by exploiting the periodic nature of the whole system. After applying a three dimensional fourier transformation to the second term the summation can be done conveniently in reciprocal space.

$$\begin{aligned} U = \quad & \sum_{i<j} \left(\sum_{|\mathbf{n}|=0}^{\infty} \frac{q_i q_j}{|\vec{r}_{ij} + \mathbf{n}|} \mathrm{erfc}(\kappa |\vec{r}_{ij} + \mathbf{n}|) \quad + \right. \\ & \left. \frac{1}{\pi L^3} \sum_{\mathbf{k} \neq \mathbf{0}} q_i q_j \frac{4\pi^2}{k^2} \exp(\frac{-k^2}{4\kappa^2}) \cos(\mathbf{k} \mathbf{r}_{ij}) \right) \quad - \frac{\kappa}{\sqrt{(}\pi)} \sum_{i=1}^{N} q_i^2 \end{aligned} \tag{49}$$

The last term of equation 49 is the so called self-term which has to be substracted in order to correct for the interaction of particles with themselves. If κ is chosen properly, the summation of the first term for all pairs can be confined to the central box. In other words, the summation of the first term in equation 49 stops at $|\mathbf{n}| = 0$. The second term is a sum over reciprocal vectors $\mathbf{k} = 2\pi\mathbf{n}/L$, how

Figure 10: Decomposition of the coulomb potential

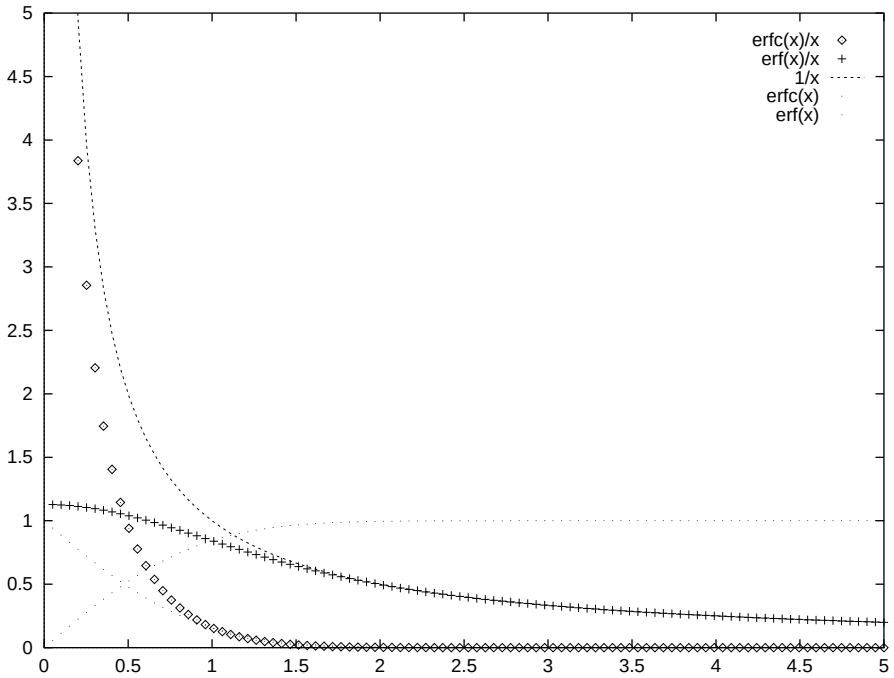

many of these have to be included depends on the value of κ. Quite a few papers have been published on the optimization of EW-calculations [28, 29]. Optimally parameterized the EW method has an execution time which scales as $N^{3/2}$ where N is the number of particles.

It could be shown that essential shortcomings arising when long range interactions get truncated can be avoided by using EW [30] and that most of the reservations concerning its use are not justified [31]. Since the advent of the particle mesh Ewald algorithm (PME) [27] — a technique which accelerates the calculation of EW considerably — the method is enjoying an increasing popularity; nevertheless, EW is still not undisputed and rarely applied within the context of free energy calculations.

3 Implementation

All the results reported in section 5 were calculated using the 27a2-version of CHARMM. Neither the separation shifted potential, nor the generalized reaction field are implemented in this version. The implementation of these concepts into CHARMM was part of this masters thesis. In the following, a brief outline of the implementation is given. The produced source code for the SSS-potential is intended to be included in upcoming versions of CHARMM, and the reader is referred to http://yuri.harvard.edu for more details on the implemented facilities for free energy calculation, as well as the general capabilities of CHARMM.

3.1 The PERT module of CHARMM

SSS was implemented as an extension of PERT, one of the CHARMM-modules for the calculation of free energy differences. PERT performs these calculation using TI, as well as PM, in the course of a single topology simulation [32] with linear λ-scaling, i.e., TI is carried out according to equation 23. The implementation of SSS was necessary to remove the drawbacks of linear λ-scaling discussed in section 2.2.5. PERT itself is implemented quite non-intrusively: the energy and dynamics routines provided by CHARMM are used without substantial changes. When the PERT command is given in a CHARMM input script, a copy is made of the current topology and force-field parameters. This has to be followed by user-supplied changes of the topology/parameters. An ENERGY (= calculate the energy) or DYNA (= run molecular dynamics) command now calculates the energy for both sets of parameters separately, and U is calculated as a function of λ according to equation 23. Efficiency is maintained by clever use of the non-bonded lists. The numerical integration is done, using the trapezoidal rule. Both windowing and slow growth are supported by PERT.

3.2 The Separation Shifted Potentials

The main task of the implementation of SSS into PERT was the change of equation 23 to

$$U(r,\lambda) = (1-\lambda)U_i(r,\lambda) + \lambda U_f(r,\lambda) \tag{50}$$

i.e., the initial and final potential energy, U_i and U_f are not anymore only functions of the particle-coordinates, and of two separate sets of constant force field parameters, but of λ as well. Thus, in the inner loop of the energy routine the equations for the potential, as well as its derivatives with respect to the coordinates and λ, had to be rewritten. For the detailed equations, see appendix A. It seemed to be appropriate not to modify the original energy routines, but rather to write a separate routine, called only when SSS is used. Therefore, the CHARMM-routines EVDW and ENBFAST were copied and renamed, and the required changes were done solely within these copies. A few lines of code were added to the book-keeping subroutines EPSUM and PERTAN of PERT which also provide the human readable output.

3.3 Generalized Reaction Field

In contrast to SSS, the GRF-potential, as given in equation 46 was implemented, by modifying the original CHARMM non bonded energy routines EVDW and ENBFAST, which was a quite straightforward task. Details will not be discussed here, since the implementation was accomplished in a rather ad hoc manner and the resulting code is not intended for incorporation into the official CHARMM-distribution.

4 Computational Details

4.1 Methods and Systems

In section 5 the results for two different sets of free energy calculations are given. The first of these sets consists of a series of calculations for different systems, carried out to verify the correct implementation of the SSS-potentials and to test their performance and accuracy when dealing with the VdWEP. The accordant results are given in section 5.1. In section 5.2 a number of calculations of the free energy of solvation of water are presented. This second set of results allows the estimation of the influence of different ways of treating the long range interactions in the context of free energy simulations of polar molecules.

The systems investigated in section 5.1 were chosen according to the following criteria: i) they should be simple enough, so that enough calculations can be performed in a reasonable amount of time; ii) they should be complex enough, so that results and findings can be generalized and applied to large and complex systems; iii) reference data from other publications as well as experimental results should be available.

Before testing the ability of the implemented method to cope with the Van der Waals endpoint problem, several simulations were carried out for non critical systems, i.e., for systems for which it is known that the VdWEP will not arise. This is done, in order to verify the principal equivalence of the results of separation shifted and linear scaling. Furthermore such calculations are essential to test the correct implementation of the code.

For all simulations either the CHARMM module PERT or PSSP, the modified version using SSS, as described in section 2.2.5 were used. Free energy differences were calculated by performing forward and backward TI, either with windowing or slow growth. The force field parameters were taken from the CHARMM22 All-Hydrogen Parameter Set for small model compounds [5].

The temperature was kept close to 300 Kelvin for all the investigated systems by using a Nose-Hoover thermostat [9] with a thermal inertia parameter of 10 kcal sec^2 mol^{-1}. Since it is the default option of CHARMM, the tapering function applied to the Coulomb potential was ASHF in most of the calculations. For the VdW-interaction, i.e., the Lennard-Jones potential, ASWI was used throughout. Another issue, common to all the calculations presented here, is the fact, that the mass of the hydrogen atoms was set to 10 amu. This provision allows the usage of a longer time step for the integration algorithm without affecting any energy results.

Next, the parameters and topologies as well as the protocols used for the free energy calculations are presented. A free energy simulation protocol is a set of data characterizing the kind, number and extent of calculations performed for a particular system. It includes the total number of time steps used for one run, the total number of forward and backward runs, the width of a window etc. In order to facilitate the legibility of the tables in section 5, the simulation protocols that were used for doing the test calculations are summarized in this chapter and each protocol is given a label. This label has the form X-Y, where X is either SG for slow growth or WI for windowing, and Y is the total number of time-steps/1000. For each system at least one forward and one backward simulation run was carried out.

Table 2 presents some of the parameters and physical quantities defining a system according to equation 38 and their abbreviations and physical units. Where necessary, these parameters will be given an index i for the initial ($\lambda = 0$) or f for the final ($\lambda = 1$) state of a transition. Instead of the Lennard-Jones parameter σ, usually $r_{min}/2$, i.e., half the the distance of the minimum of the potential curve to the origin, is given, since it is specified in this form in the CHARMM parameter files. The LJ-parameter σ — as used in equation 38 — is recovered through $\sigma = 2r_{min}/2^{1/6}$. For the evaluation of ϵ and σ for pairs of different atoms,

Table 2: The parameters, abbreviations and units

name	symbol	unit
number of particles	N	-
volume	V	Å^3
density	ρ	Å^{-3}
length	l	Å
mass	m	amu (1.6603×10^{-27} kg)
time	t	ps (10^{-12} sec)
energy	E	kcal/mol
charge	q	e_0 (1.6021×10^{-19} C)
time step for integration	δt	ps (10^{-12} sec)
LJ, energy parameter	ϵ	kcal/mol
LJ, distance parameter	σ	Å
LJ, equilibrium distance	$r_{min}/2$	Å
force constant for bonds	k^b	kcal/(mol Å^2)
equilibrium bond length	b^0	Å
cutoff radius	r_c	Å
inner cutoff radius	r_i	Å

CHARMM uses the following mixing rules

$$\sigma_{ab} = \frac{1}{2}\left(\sigma_a + \sigma_b\right) \tag{51}$$

$$\epsilon_{ab} = \sqrt{\epsilon_a \times \epsilon_b} \tag{52}$$

The partial charges are given in units of elementary charge e_0. In all the equations involving the Coulomb potential the required conversion factor to obtain the energy in kcal/mol will be omitted to increase the legibility.

4.1.1 One-dimensional Harmonic Oscillator

The topology of this very simple system, henceforth called 1DHO, is shown in figure 11. The Hamiltonian of the 1DHO is simple enough so that the configurational integral can be evaluated by numerical quadrature. Mathematica[33] was used for this task, thus providing a rigorous calibration for the free energies calculated with TI or equivalent methods. The free energy difference between two 1DHOs, characterized by different values for some force-field parameters, can be calculated with little computational effort. Therefore, calculations were carried out to test the correct implementation of the code for all combinations of the separation shifted potential with different tapering functions and with several values for the shifting parameters δ_v and δ_e.

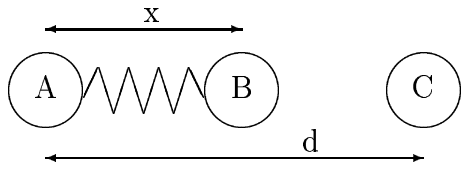

Figure 11: The one dimensional harmonic oscillator

The force field parameters are given in table 3. The distance $d = 5$Å between the particles labeled A and C, respectively, is held constant during the simulation. Thus, the only moving particle is the one labeled B. By setting the initial velocities accordingly, the motion of B is confined to one dimension, leaving the system only a single degree of freedom. Between particles B and C there are Lennard Jones as well as Coulomb interactions. Between A and B a harmonic bond potential is defined, whereas A and C do not see each other. The cutoffs r_i and r_c, are set to 7 and 8 Å, respectively and a time-step of 0.001 ps is used. The Hamiltonian of the system, as given in equation 53, is a function of x, the distance between A

and B, and of course λ.

$$
\begin{aligned}
H(x,\lambda) &= (1-\lambda)H_i(x,\lambda) + \lambda H_f(x,\lambda) \\
H_i(x,\lambda) &= k_i^b(x-b_i^0)^2 + \frac{q_i^B q_i^C}{\sqrt{(d-x)^2+\delta_e\lambda}} + \\
&\quad 4\epsilon_i\left\{\frac{\sigma_i^{12}}{((d-x)^2+\delta_v\lambda)^6} - \frac{\sigma_i^6}{((d-x)^2+\delta_v\lambda)^3}\right\} \qquad (53) \\
H_f(x,\lambda) &= k_f^b(x-b_f^0)^2 + \frac{q_f^B q_f^C}{\sqrt{(d-x)^2+\delta_e(1-\lambda)}} + \\
&\quad 4\epsilon_f\left\{\frac{\sigma_f^{12}}{((d-x)^2+\delta_v(1-\lambda))^6} - \frac{\sigma_f^6}{((d-x)^2+\delta_v(1-\lambda))^3}\right\}
\end{aligned}
$$

Table 3: Parameters for the one dimensional harmonic oscillator

parameter	unit	initial value	final value[a]
m(A,B,C)	amu	12.0	—
$q(B)$	e_0	0.5	0.5
$q(C)$	e_0	-0.5	-0.8
b_0	Å	1.526	0.300
k_b	kcal/mol/Å^2	260.0	80.0
$\epsilon(B)$	kcal/mol	-0.175	—
$\epsilon(C)$	kcal/mol	-0.175	—
$r_{min}(B)$	Å	2.19161	—
$r_{min}(C)$	Å	2.19161	—

[a]If no final value is given, initial and final values are identical.

Table 4: The simulation protocol for all calculations for the 1DHO

label	N_{prod}[a]	N_{eq}[b]	N_{fwd}[c]	N_{bwd}[d]
SG-600	100000	20000	3	3
SG-2000	100000	20000	10	10

[a] number of production steps for one single fwd or bwd run
[b] number of equilibration steps for one single fwd or bwd run
[c] number of forward runs
[d] number of backward runs

4.1.2 Ethane and Methanol

The free energy difference of solvation between ethane and methanol, although still being a rather simple test calculation, already contains most of the characteristics typical for more complex applications. It was the first widely known free energy calculation [34] and can serve as an example of the use of a thermodynamic cycle as well as of an alchemical mutation. The mutation involves changes in VdW as well as in electrostatic interactions, and — though frequently omitted — also internal degrees of freedom. Reference data, i.e., experimental values as well as results of other calculations are available. All this leads to its use as a *de facto* benchmark for algorithms used in free energy calculations. The main reason for the investigation of this system is to test the correctness of the implementation since the ethane to methanol mutation can be considered unproblematic in terms of the VdWEP. Additionally some test-calculations were carried out, using different TFs in order to determine their influence on the results.

For the mutation of ethane to methanol simulations were performed in the gas-phase, i.e., for one single ethane/methanol hybrid molecule ($\Delta A_{gas} \equiv \Delta A_3$ in figure 1) and in aqueous solution — one ethane/methanol hybrid in 122 TIP3P water molecules ($\Delta A_{solv} \equiv \Delta A_4$ in figure 1). Neither of these quantities can

be determined experimentally. However, since A is a state function, the relation $\Delta\Delta A = \Delta A_3 + \Delta A_4 = -\Delta A_1 - \Delta A_2$ can be used to compare the obtained results to experimental reference data [40] (see figure 1).

PERT performs the free energy calculations as *single topology simulations* [32]. The number of atomic sites has to be the same for both configurations of the hybrid molecule. At the methanol end of the transition two dummy sites take the place of two methyl hydrogens.

For the force field parameters of ethane and methanol as well as TIP3P the reader is referred to the above mentioned CHARMM parameter set. The starting configuration for all the following simulations was obtained by placing an ethane molecule into an equilibrated box of side length 15.5516 Å, containing 125 TIP3P molecules. Those water molecules that did significantly overlap with ethane were removed, and the resulting system of 122 TIP3P and one ethane was equilibrated for 20 pico-seconds once more. Due to the rather small box-size, r_c and r_i were set to 7.6 and 6.0 Å, respectively. The time-step used by the integration algorithm was 0.001 ps.

Table 5: The simulation protocols for ethane → methanol in the gas phase

label	N_{prod}[a]	N_{eq}[b]	N_{fwd}[c]	N_{bwd}[d]
SG-720	100000	20000	3	3
SG-1200	100000	20000	5	5

[a] number of production steps for one single fwd or bwd run
[b] number of equilibration steps for one single fwd or bwd run
[c] number of forward runs
[d] number of backward runs

Table 6: The simulation protocols for ethane → methanol in aqueous solution

label	N_{prod}[a]	N_{eq}[b]	N_{win}[c]	N_{fwd}[d]	N_{bwd}[e]	N_{eq1}[f]
WI-408	8200	2000	20	1	1	50000
WI-420	8000	2000	21	1	1	50000
WI-600	20000	10000	10	1	1	10000
WI-1008	20000	4000	21	1	1	50000
WI-1260	8000	2000	21	3	3	50000

[a] number of production steps per window
[b] number of equilibration steps per window
[c] number of windows per run
[d] number of forward runs
[e] number of backward runs
[f] number of equilibration steps at $\lambda = 0$ and $\lambda = 1$

4.1.3 Neon in Aqueous Solution

The free energy of solvation of neon in water is the first example given here for a calculation where the VdWEP is of importance. Since here the interactions with one particle are turned off completely, all the problems associated with the VdWEP can be expected to arise. Three different approaches are made to compare the performance of PSSP and linear scaling:

NLI linear TI with windows for $\lambda = 0.025, 0.075, \ldots, 0.975$

NEX linear TI up to $\lambda = 0.9$, followed by additional calculations at λ-values between 0.9 and 0.998 and calculation of ΔA between $\lambda = 0.9$ and $\lambda = 1.0$ as described in section 2.2.5

NSS TI with PSSP for $\lambda = 0.0, 0.05, \ldots, 1.0$

By avoiding to simulate the system in the state $\lambda = 1$, as done in case NLI, the problem of floating point overflows can be readily avoided without reducing the time-step. Attempt NLI is only performed, in order to estimate the error introduced by proceeding in this manner. Attempt NEX, on the other hand, should give correct results for the free energy difference. So this method was employed to have an independent reference value to which the result obtained with PSSP can be compared. There is also a second reason for employing the method of case B: The performance, that is, the relation between the correctness of the results and the consumed CPU time can be estimated and compared to case NSS.

The system used for the calculations of the free energy of solvation of neon was basically a cubic box of side length 18.856 Å containing 215 TIP3P and one neon molecule. The state $\lambda = 0$ corresponds to the neon particle, being entirely present, whereas for $\lambda = 1$ the interactions between neon and the solute are completely turned off, leaving 215 TIP3P and one ideal-gas neon particle. Just as for the ethane $\rightarrow$ methanol system the initial configuration was constructed by placing a single neon atom into a box with, in this case, 216 pre-equilibrated TIP3P water molecules. Since the VdW-radius of neon and water are quite similar, just one TIP3P was replaced by the neon, resulting in a system of 215 TIP3P and one neon molecule. Starting from this configuration, the particles were assigned random velocities, and by performing several simulation runs over different time intervals a number of different restart-files were produced for the following free energy calculations. If not indicated otherwise a time step of 0.002 ps was used. The cutoff r_c as well as the inner cutoff r_i were set to 8.5 Å, resulting in a crude truncation of the Coulomb interactions. The force field parameters of neon are merely three numbers: the LJ parameters $r_{min}/2 = 1.53$ Å, $\epsilon_0 = -0.086$ kcal/mol and the mass $m = 20.179$ amu. The force field-parameters for TIP3P are given in section 4.1.4. The simulation-protocols are detailed in table 7.

Table 7: The simulation protocols for neon in aqueous solution

label	N_{prod} [a]	N_{eq} [b]	N_{win} [c]	N_{fwd} [d]	N_{bwd} [e]	N_{eq1} [f]
WI-1120	24000	4000	20	1	1	8000
WI-760	3000	1000	19	5	5	1000
WI-168	3000	1000	21	1	1	25000
WI-840	3000	1000	21	5	5	1000
WI-1470	4500	2500	21	5	5	2500
WI-1680	6000	2000	21	5	5	2000

[a] number of production steps per window
[b] number of equilibration steps for each λ-value
[c] number of windows per run
[d] number of forward runs
[e] number of backward runs
[f] number of equilibration steps at $\lambda = 0$ and $\lambda = 1$

Table 8: The protocols for PERT-NEX calculations

λ	0.9	0.95	0.98	0.99	0.995	0.998
δt [fs]	2	2	1	0.5	0.25	0.25
time-steps/window	1000	1000	2000	4000	8000	8000
number of windows	50	100	100	100	100	22

In table 8 the protocol used for the additional calculations required in NEX for the extrapolation of $\langle \partial U/\partial \lambda \rangle_\lambda$ for $\lambda = 0.9 - 1.0$ is given. The number of windows calculated for each λ-value, as well as the time-step used thereby, are given. Since for simulations with λ being so close to the critical value of 1 — even when smaller time-steps are used — floating point errors can be expected

to arise frequently, lots of rather small windows are calculated rather than a few larger ones, minimizing by that the amount of futile calculation effort.

4.1.4 Water in Aqueous Solution

The investigations performed for water are twofold: Just like for the neon-system calculations are done, employing linear scaling, linear scaling in combination with extrapolation and separation shifted scaling. The three methods were labelled accordingly:

WLI linear scaling of λ, avoiding the calculation of $\langle \partial U/\partial \lambda \rangle$ at $\lambda = 1$

WEX linear scaling of λ in combination with extrapolation of $\langle \partial U/\partial \lambda \rangle$ for $\lambda \to 1$

WSS PSSP

For WLI and WSS the VdW and electrostatic interactions were turned off simultaneously, whereas for WEX two separate simulations had to be performed since the extrapolation scheme is only valid for VdW-interactions. The performance and the accuracy of the results were compared for the three methods. In this case, as opposed to the neon system, there are electrostatic interactions between the test particle and the solvent. and for the WSS-case SSS is applied to the VdW as well as the electrostatic interactions.

In addition to the SSS-approach, for coping with the VdWEP the second main topic of this masters thesis is the investigation of the dependence of free energy calculation results on the treatment of long range interactions. Essentially this amounts to a comparison of results obtained with different TFs, with results obtained with EW. Thereby the present analysis remains confined to polar molecules in contrast to ionic solutions which have been already studied thoroughly in this respect. For water three different systems are set up: a cubic box with a side-length of 18.856 Å containing 216 water molecules combined with a

cutoff of 8 Å as well as a cubic box with a side-length of 24.9434 Å containing 500 water molecules, combined with a cutoff of either 10 or 12 Å.

Table 9: Parameters for the three different water systems

number of TIP3Ps	216	500	500
box-length	18.856	24.9434	24.9434
r_i	7.0	8.0	10.0
r_c	8.0	10.0	12.0

Table 10: The simulation protocols for water

label	N_{prod}[a]	N_{eq}[b]	N_{win}[c]	N_{fwd}[d]	N_{bwd}[e]	N_{eq1}[f]
WI-980	20500	4000	20	1	1	50000
WI-1008	20000	4000	21	1	1	50000
WI-912	20000	4000	19	1	1	50000

[a] number of production steps per window
[b] number of equilibration steps for each λ-value
[c] number of windows per run
[d] number of forward runs
[e] number of backward runs
[f] number of equilibration steps at $\lambda = 0$ and $\lambda = 1$

In order to get results comparable with already published data, the actual free energy calculations are performed in two steps: First the electrostatic interactions of the test particle are turned off and in a second run the VdW-interactions. The simulation protocols for water are given in table 10. Since free energy components (as opposed to the total free energy difference) depend on the details of the simulation path [35], the terms "electrostatic" and "van der Waals" free en-

Table 11: The protocols for the PERT-WEX calculations

λ	0.9	0.95	0.97	0.98	0.99	0.995
δt [fs]	2	2	1	0.5	0.5	0.5
time-steps/window	4000	4000	8000	16000	16000	16000
number of windows	10	15	15	15	15	15

Table 12: Force field parameters for TIP3P water

parameter	value	
m(H)	10.0	amu
m(O)	15.9994	amu
d(O-H)	0.9572	Å
d(H-H)[a]	1.5139	Å
$q(O)$	-0.834	e_0
$q(H)$	0.417	e_0
$\epsilon(O)$	-0.152073	kcal/mol
$\epsilon(H)$	-0.046	kcal/mol
$r_{min}/2(O)$	1.76825	Å
$r_{min}/2(H)$	0.2245	Å

[a]Since the SHAKE algorithm was used to hold the bond angle constant, the H-H distance is given, rather than the equilibrium bond angle

ergy "contributions" (or "components") serve primarily as a convenient label. However, it is reasonable to expect and can also be shown that the bulk of the electrostatic contribution to the overall free energy difference is indeed contained

in the result obtained in the first step [36] (switching on (off) the charges of the test water).

In all calculations, the CHARMM modified TIP3P water model was used [37]; the force field parameters are listed in Table 12. The variant used in CHARMM has additional LJ-sites on the hydrogen positions so that it can be used in RISM calculations; however, it was shown that the properties of the two models are practically indistinguishable [38]. If not indicated otherwise, the time-step was set to 0.002 ps.

4.2 Estimation of Error-Bars

The calculation of error-bars within the context of free energy simulations is no straightforward task and there seems to be no general agreement in the literature on this topic. The statistical error — a consequence of the finite length simulations — can be estimated by calculating the standard-deviation of several independent simulation runs, or subsets of one longer run. On the other hand it is generally agreed that the difference between the results obtained with forward and backward simulations can serve as a measure for the error made due to insufficient equilibration of one λ-state (window), and, thus, to a lack of reversibility of the simulated transition.

Here the first kind of calculation was used to get an estimation for the actual error. If not indicated otherwise the free energy differences are given as: $\Delta A \pm \sigma$ in units of kcal/mol where σ is the standard deviation of n simulation runs or n subsets of one longer run, calculated as

$$\sigma = \frac{1}{n}\sqrt{\sum_{i}^{n}\left(\Delta A_i - \overline{\Delta A}\right)^2} \tag{54}$$

For protocols including more than one forward and backward simulation each forward or backward simulation provided one ΔA_i. In cases with just one forward and one backward simulation the ΔA_i were calculated for subsets of 4000 time-

Figure 12: Calculation of the free energy of solvation of water, protocol is WI-1008 in this case, The standard-deviation — as calculated according to equation 54 — is given as a function of the sample-length

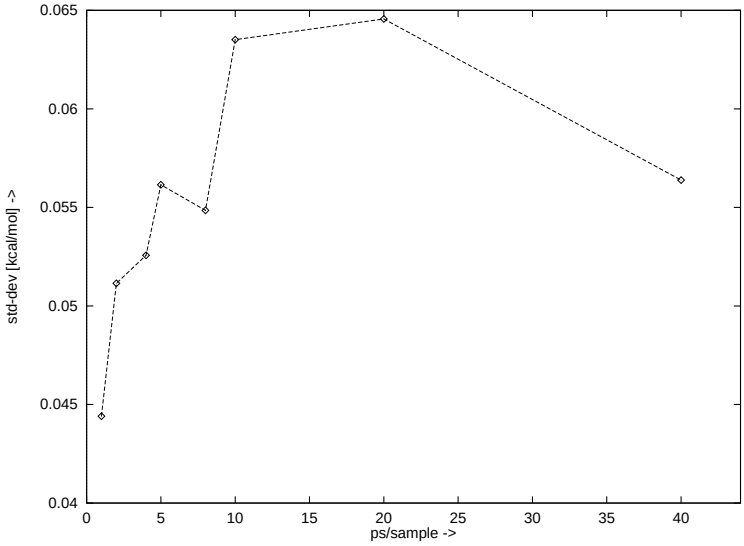

steps. As can be seen in figure 12 this number can be assumed to be large enough to exclude any bias of the error by auto-correlation effects.

5 Results and Discussion

5.1 Verification of the Implementation

5.1.1 Uncritical Systems

One-dimensional Harmonic Oscillator Calculations were performed for all the implemented TFs with Mathematica, with PERT and with PSSP, employing different shifting parameters δ_v and δ_e. Agreement between the results obtained with PERT and PSSP for the various TFs, as well as δ_v and δ_e-values, provides a necessary criterion for the correct implementation of the PSSP algorithm.

For the system described in section 4.1.1, but with uncharged particles Boresch and Karplus [32] report a ΔA of -1.92 kcal/mol, using PERT in combination with ASHF and the protocol SG-2000. Numerical integration of the Hamiltonian with Mathematica gives the same result. With PSSP, SG-600 as protocol and $\delta_v = 5$, 10 or 15 Å^2 a ΔA of -1.91 kcal/mol was obtained for all three values of δ_v.

For all systems investigated ΔA calculated with PERT and with PSSP and $\delta_v = \delta_e = 0$, were found to be identical, as they must, since in this case PSSP and PERT follow the same simulation path. For finite values of the shifting parameters, the difference between PERT and PSSP results was always below one percent and the corresponding error-bars are negligibly small.

Figure 13 shows results for the system described in section 4.1.1 with invariable partial charges. Free energy differences for different TFs as a function of δ_v and δ_e are shown. In figure 14 results for the same system with changing partial charges are shown. One clearly sees that ΔA does not depend on the value of δ_v or δ_e since for all systems the ΔAs are practically identical and the small deviations from the overall mean value are always of the same order of magnitude as the standard deviations. Apart from this finding a noticeable feature are the rather large differences between the results for different TFs. The reasons for this effect will be discussed in section 5.2. The essential finding, expressed by the results

Figure 13: ΔA for the 1DHO for different TFs as function of δ_v and δ_e (with constant partial charges)

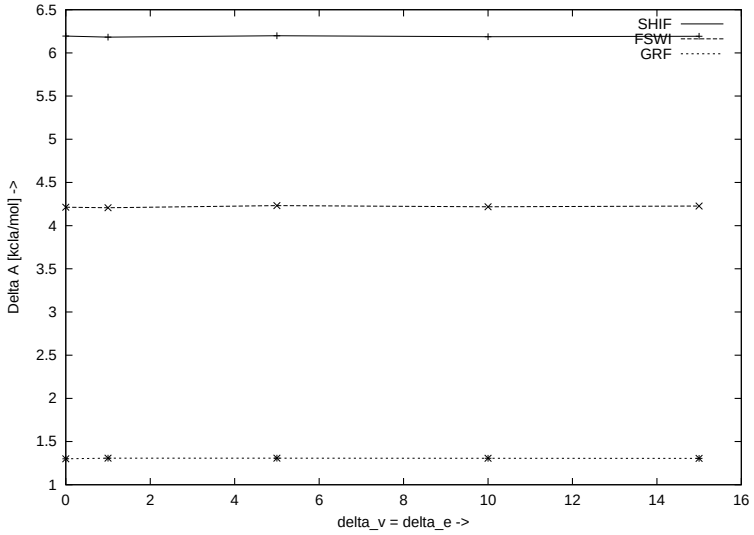

Figure 14: ΔA for the 1DHO for different TFs as function of δ_v and δ_e (with changing partial charges)

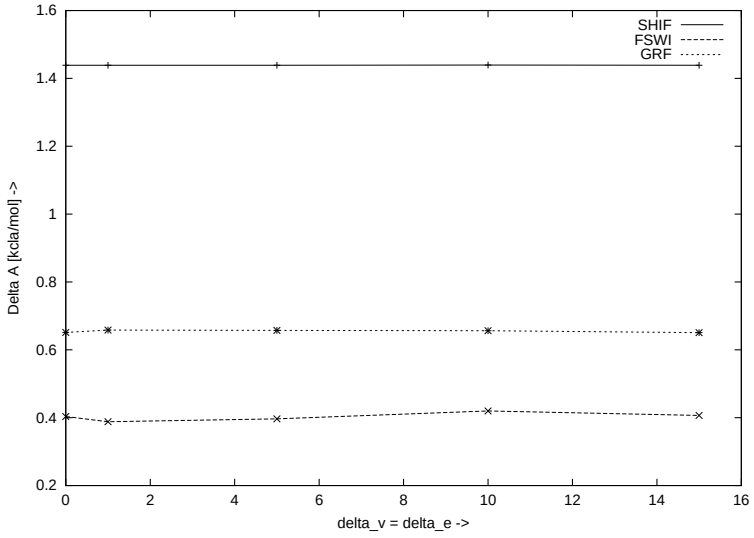

presented in this section, is the correct implementation of the SSS-potential, its derivatives and book-keeping routines.

Free Energy Difference of Solvation Between Ethane and Methanol The difference between the free energies of solvation for ethanol and methanol were calculated with PERT as well as with PSSP. Figure 15 shows the free energy results of calculations in the gas phase as a function of δ_v and δ_a for several TFs. The findings and conclusions are essentially the same as for the 1DHO: ΔA shows no systematic variation with increasing shifting parameters. and the deviations from the over-all mean are not larger than the average standard-deviation. Compared to the 1DHO results, the variations are larger. This is to be expected, since the considered system is more complex, resulting in larger statistical fluctuations. Table 13 finally compares experimental data and computed free energies reported

Figure 15: ΔA for ethane $\rightarrow$ methanol as a function of the shifting parameters δ_{vdw} and δ_{el} for different TFs

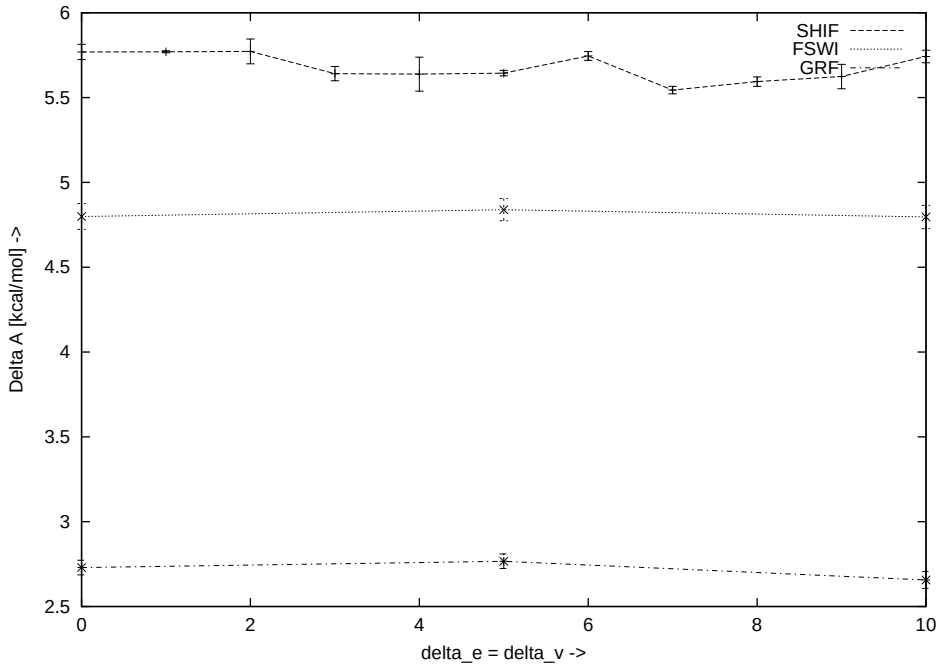

by Boresch and Karplus [32, 39] with results obtained with PSSP as well as with PERT for $\Delta A_{gas} + \Delta A_{solv}$. Once again the difference between results, obtained with different algorithms is well below the respective standard-deviation.

Table 13: Free energy of solvation difference between ethane and methanol

algorithm	protocol (gas/solv)	ΔA_{gas}	ΔA_{solv}	$\Delta\Delta A$
PERT	SG-720/WI-480	5.6 ± 0.2	-2.8 ± 0.2	-8.4
PERT[a]	SG-2000/WI-600	5.7 ± 0.1	-2.8 ± 0.9	-8.5
PSSP[b]	SG-720/WI-1260	5.8 ± 0.1	-2.7 ± 0.2	-8.4
exp [c]				-6.9

[a] Ref. [32, 39]
[b] $\delta_v = \delta_e = 5$ Å^2
[c] Experimental value[40]

Ethane has got two atomic sites more than methanol, i.e., the mutation involves the conversion of two hydrogen atoms into so called dummy-sites.[‖] Mass and bonded parameters of these dummy sites remain unchanged,[**] whereas the electrostatic and the VdW interactions are turned off (on). Thus, when performing this mutation in solution, this system could be expected to behave *not* non critical at all since the necesarry condition for the VdWEP is given. However, it can even be studied with linear TI, since for this system the shape of $\langle \partial U/\partial\lambda \rangle$ as a function of λ is sufficiently well behaved, so that the numerical integration gives reliable results. The VdWEP does not arise, because the hydrogen dummy atoms are shielded almost entirely by the VdW-sphere of the carbon/oxygen atom they are bound to. Rather big fluctuations of ΔA will occur, however, as soon

[‖] cf. figure 3b in Ref. [32]
[**] It is common practice to change the bond-lengths in the course of the mutation; in this case, however correction terms have be added to the resulting free energy difference [32]

as the simulations are performed at $\lambda = 0$ or $\lambda = 1$. Thus, in the calculations with PERT, the end-states have to be avoided by using an appropriate series of λ-values. For the PERT-results in table 13, for example, 20 windows with $\lambda = 0.025, 0.05, \ldots, 0.975$ were used.

The results of this and of the precedent section can be summarized as to prove the aequivalence of the results obtained with PERT and PSSP and in particular the correct implementation of SSS into CHARMM.

5.1.2 Particle Insertions

In the last two sections the implementation of SSS was tested for non-problematic systems. In the following, the ability of SSS to circumvent the VdWEP will be tested for two critical calculations: The first one, involving only separation shifted VdW-interactions, is the calculation of the free energy of solvation of neon in water. The second is the free energy of solvation of a single water molecule in aqueous solution.

Free Energy of Hydration of Neon In table 14 the results are given for the calculations performed according to the three methods described in section 4.1.3. Additionally reference data and the experimental result are given. The result for case NLI is quite poor, while the results, obtained with method NEX and NSS both agree well with the reference data of Zacharias [3]. The experimental result is reproduced less well. On the other hand, methods NEX and NSS and the result of Zacharias are equally poor in this respect. Thus, it can be assumed that the force field rather than the method is to blame. The unsatisfactory result for the NLI-protocol comes not surprisingly. Figure 16 shows the accordant values of $\langle \partial U/\partial\lambda \rangle$. Since $\langle \partial U/\partial\lambda \rangle$ undergoes rapid changes in the vicinity of $\lambda = 1$ — actually it diverges — the contribution to the integral between $\lambda = 0.95$ and $\lambda = 1.0$ gets obviously underestimated by far. For $\lambda = 0 - 0.9$ the NEX and NSS protocols involved the same number of time-steps for the same λ-values. For NEX additional and — as indicated in table 8 — quite lengthy calculations were performed for windows at $\lambda = 0.9, 0.95, 0.98, 0.99, 0.995$ and 0.998. Although with method NEX and NSS essentially equal results are obtained, PSSP is definitely the more efficient approach, since the amount of CPU time required to get a result of equal accurateness is much higher for the extrapolation method. Moreover, the errorbar indicated for method NEX is probably underestimated. To see this, the protocol used in case NEX has to be considered: In table 15 the

Table 14: Annihilation of Neon in water; results for different algorithms

method[a]	protocol	ΔA
NLI	WI-1120	-0.06 ± 0.05
NEX	WI-760[b]	-1.74 ± 1.04
NSS	WI-840	-1.78 ± 0.20
ref[c]	WI-168	-1.91 ± 0.7
exp[d]		-2.39

[a] see text for explanation of the symbols

[b] This protocol covers only the simulations up to $\lambda = 0.9$. See text and section 4.1.3 for details on the extrapolation.

[c] Zacharias[3] used PSSP and a cutoff of 9.5 Å for 192 SPC/E water molecules

[d] experimental result[41]

results for simulations up to $\lambda = 0.9$ are presented for case NEX. The errorbars for this contribution to ΔA are quite small. For the rest of the mutation, however, i.e., for $\lambda = 0.9 - 0.998$ the situation becomes quite unpleasant in this respect, as revealed by table 16 and figure 17, respectively. Especially the figure clearly demonstrates the high uncertainty of these calculations. For simulations at values of λ near one, fluctuations of the calculated $\langle \partial U/\partial \lambda \rangle$ become very large and the mean values converge very slowly, not to mention the very small time-steps required to do these calculations, resulting in exorbitant consumption of CPU time. An example for the slow convergence of a single value of $\langle \partial U/\partial \lambda \rangle$ is given in figure 18. Each point in the figure represents the result of a 2 ps-subset of a 90 ps-simulation of the state $\lambda = 0.995$. Using the values for $\langle \partial U/\partial \lambda \rangle$, given in table 16 and Mathematica's[33] built-in function *Fit*, a least square fit was calculated to get the parameters of a function as given in equation 42. This function

Figure 16: $\langle \partial U/\partial \lambda \rangle$ for neon in aqueous solution with the NLI-protocol.

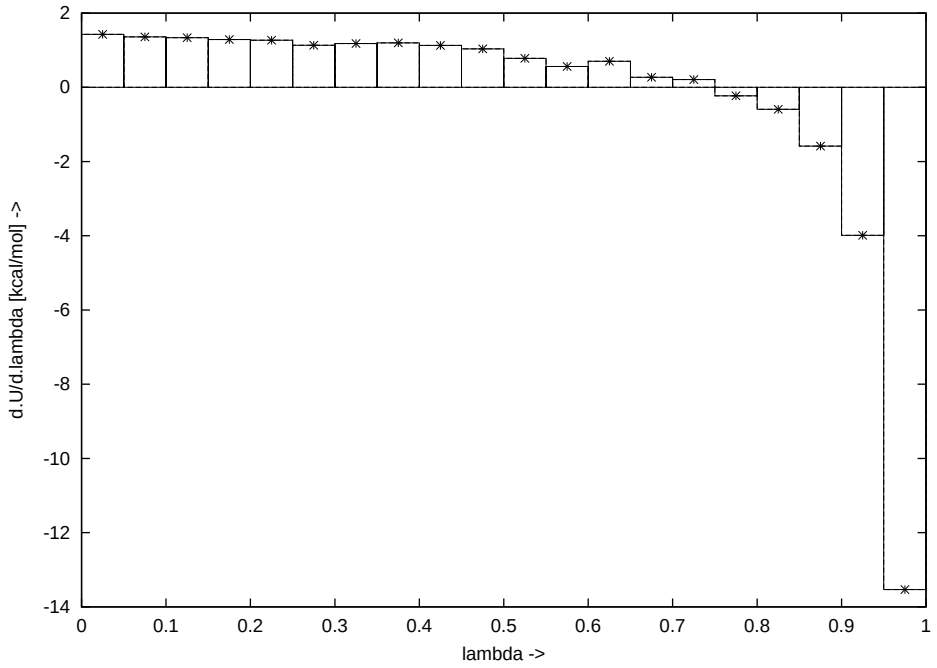

was integrated analytically between $\lambda = 0.9$ and 1.0 and the result was added to the ΔA for $\lambda = 0-0.9$. The evaluation of the error-bar for this kind of calculation is not a straightforward task. Here, the numerous results $\langle \partial U/\partial \lambda \rangle$ calculated for each λ-value between 0.9 and 0.998 were divided into five subsets for each λ. For each of these five subsets, a seperate least square fit was established, resulting in five estimates for ΔA for $\lambda = 0.9 - 1.0$. The mean value of ΔA for $\lambda = 0.0 - 0.9$ was added to each of these five estimates and the rather high standard-deviation of 1.04 kcal/mol was calculated for the resulting five values of the total ΔA.

Additional calculations were performed, in order to estimate the dependence of the PSSP-results on simulation length and the parameter δ_v. The results are shown in table 17 and 18. All results are found within a range of approximately 0.3 kcal/mol. That is, the calculated free energies seem to be relatively insensitive to variations of the shifting parameter, and there is no evidence that longer simulation times than the 330ps used by Zacharias would change the results.

The final outcome of all of the above calculations is that, when applying PSSP in free energy calculations, high fluctuations and slow convergence of the results due to the VdW-endpoint problem can be successfully circumvented. Zacharias found that the precision of the results declines with increasing δ_v. A comparison of the results for case NLI and NSS in table 14 as well as those those of table 18, support this observation. However, the overall value of the standard deviation does never exceed a range of reasonable size.

Figure 17: Annihilation of Neon; $\langle \partial U / \partial \lambda \rangle$ and its standard deviation for $\lambda \to 1$

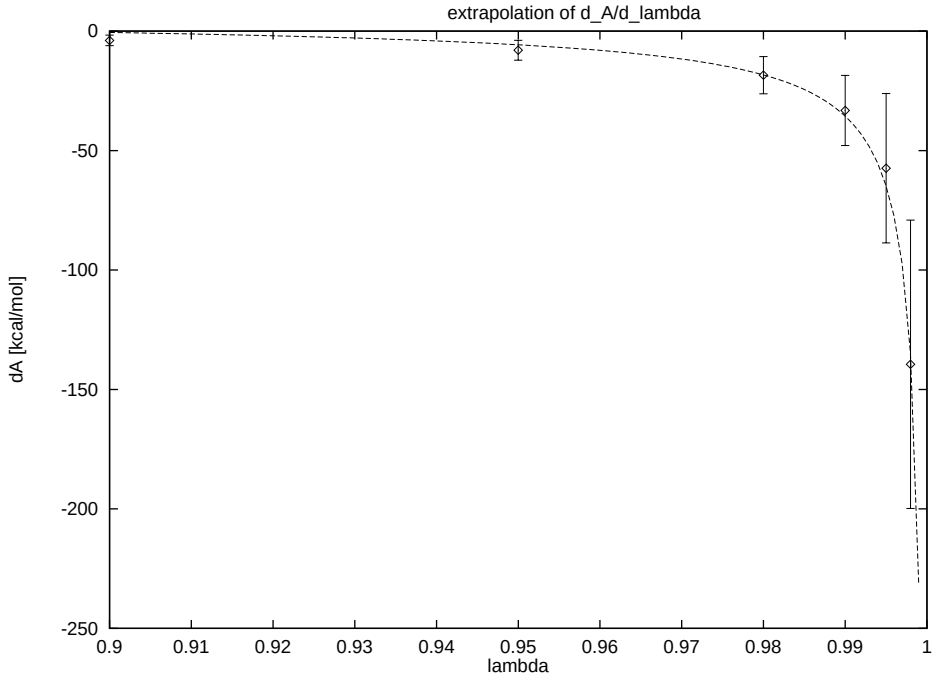

Figure 18: Annihilation of Neon; $\langle \partial U/\partial \lambda \rangle$ calculated for windows of 2 ps (8000 steps) for $\lambda = 0.995$

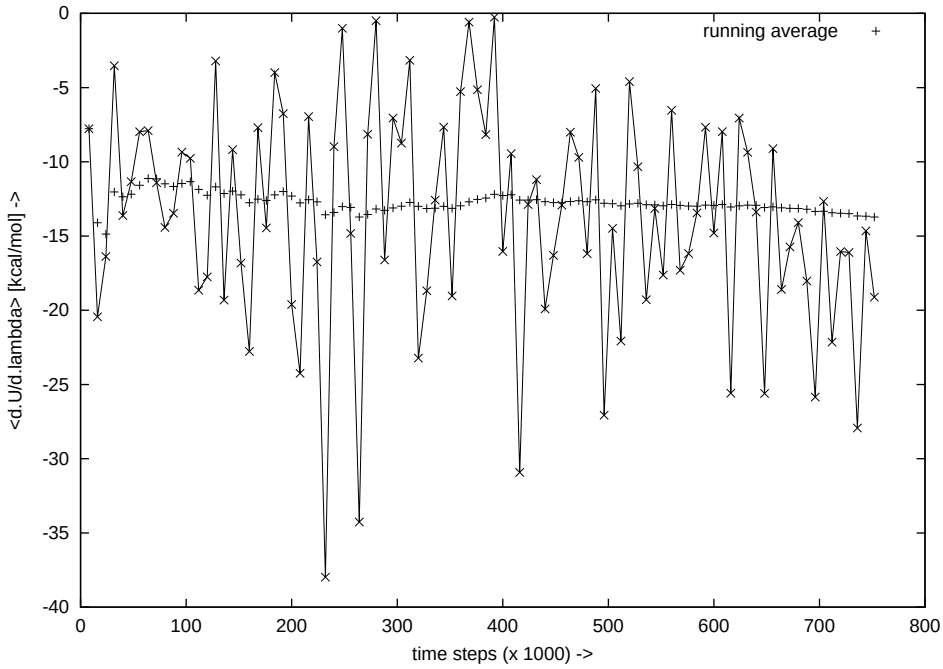

Table 15: Annihilation of Neon; PERT-results for $\lambda = 0.0 - 0.9$

protocol	ΔA
SG-1000	0.63 ± 0.09
WI-540	0.56 ± 0.06

Table 16: Neon; $\langle \partial U/\partial \lambda \rangle$ for $\lambda = 0.9 - 0.995$

λ	t_{sim} [ps]	$\langle \partial U/\partial \lambda \rangle$
0.900	100	-0.93 ± 0.53
0.950	190	-1.91 ± 0.99
0.980	190	-4.40 ± 1.86
0.990	190	-7.93 ± 3.51
0.995	190	-13.7 ± 7.47
0.998	44	-33.3 ± 14.41

Table 17: PSSP calculations for neon; dependence of the results on simulation length

protocol	ΔA
WI-168[a]	1.91 ± 0.17
WI-840	1.78 ± 0.20
WI-1470	1.61 ± 0.25
WI-1680	1.86 ± 0.21

[a] Zacharias et al [3]

Table 18: Neon; dependence of the results on separation parameter δ_v

δ_v [a]	ΔA
5	1.78 ± 0.20
10	1.87 ± 0.26
15	1.62 ± 0.30

[a] The simulation protocol is WI-840 throughout

Free Energy of Hydration of Water This section is concerned with the verification of PSSP, and the demonstration of its superior performance compared to other approaches to circumvent the VdWEP. In contrast to the preceeding section, here a system including electrostatic interactions is investigated. Additional results for the free energy difference of hydration of water will be presented in Sect. 5.3, where the influence of the treatment of electrostatic interactions on the results of free energy calculations is investigated. The free energy of solvation of water was calculated and investigations proceeded in a similar manner as it was done for neon. Zacharias found a value of 5 $Å^2$ to be sufficient to suppress negative effects of the VdWEP, yet small enough not to lead to sizeable fluctuations of the results. Since in all calculations this far no evidence was found, to doubt this value, all the PSSP-results for the free energy of solvation of water are calculated with the parameters $\delta_v = \delta_e = 5$ $Å^2$. The influence of varying cutoff radius and the usage of different TFs will be discussed in section 5.2. For all calculations discussed here, the small (N = 216) water box was used and the cutoff was set to 8 Å while ASHF was used as TF. In table 19 the free energy

Table 19: Free energy of solvation of water, results for calculations using PERT and PSSP

method	protocol	ΔA
WLI	WI-980	9.26 $\pm$ 0.06
WEX	WI-1008 + WI-912	8.20 $\pm$ 0.30
WSS	WI-1008	8.10 $\pm$ 0.10

results for the three methods indicated above are given. Again the result for WLI is the poorest, while the results calculated with extrapolation and SSS are equal within the given error-bars. The reason for WEX, as well as WSS, being quite

far off the experimental result [40] of $\Delta A = 6.32$ kcal/mol will be discussed in section 5.2. For the time being the relevant findind is that the two methods give practically the same value for the free energy difference. Concerning the number of time-steps required, to get a result of compareable quality, the extrapolation method performs for water even worse than for neon. In addition to the 960000 additional time-steps used for extrapolation a further complication arises: The electrostatic interactions have to be turned off in a separate simulation since the extrapolation approach of Simonson is not valid for potentials of the form $\frac{1}{r}$. Probably one could perform the two simulation runs for turning off VdW and electrostatic interactions separately in less than twice the time it can be done in a concerted fashion. Nevertheless, it appears to be clear that PSSP outperforms the extrapolation algorithm by far in the price/performance relation as well as the precision of the results. In spite of using more than twice the simulation time, the error-bar of 0.3 kcal/mol for the WEX result given in tabel 19 is definitely higher than the 0.1 kcal/mol given for the WSS result.

5.2 Effects of the Truncation of Long-Range-Interactions

In table 20 and 21 results for the VdW- and the electrostatic contribution to the free energy of solvation of water are given. ΔA_{VdW} does not show any systematic variations depending on cutoff sizes or tapering functions. The overall mean value for ΔA_{VdW} was -1.73 kcal/mol, and the corresponding standard deviation turned out to be as low as 0.033 kcal/mol.

The free energy difference ΔA_{el}, resulting from turning off the coulomb interactions of one TIP3P, however, turns out to be extremely sensible to the choice of tapering function as well as the cutoff radius. In Figure 19 ΔA_{el} as a function of the cutoff radius is presented for different tapering functions. When using GSWI or EW, the results remain practically the same when rising the cutoff from 8 to 12 Å. The actual values for the free energy difference are — within the error-

Figure 19: Electrostatic contribution to the free energy of solvation of water; results for different cutoffs and tapering functions

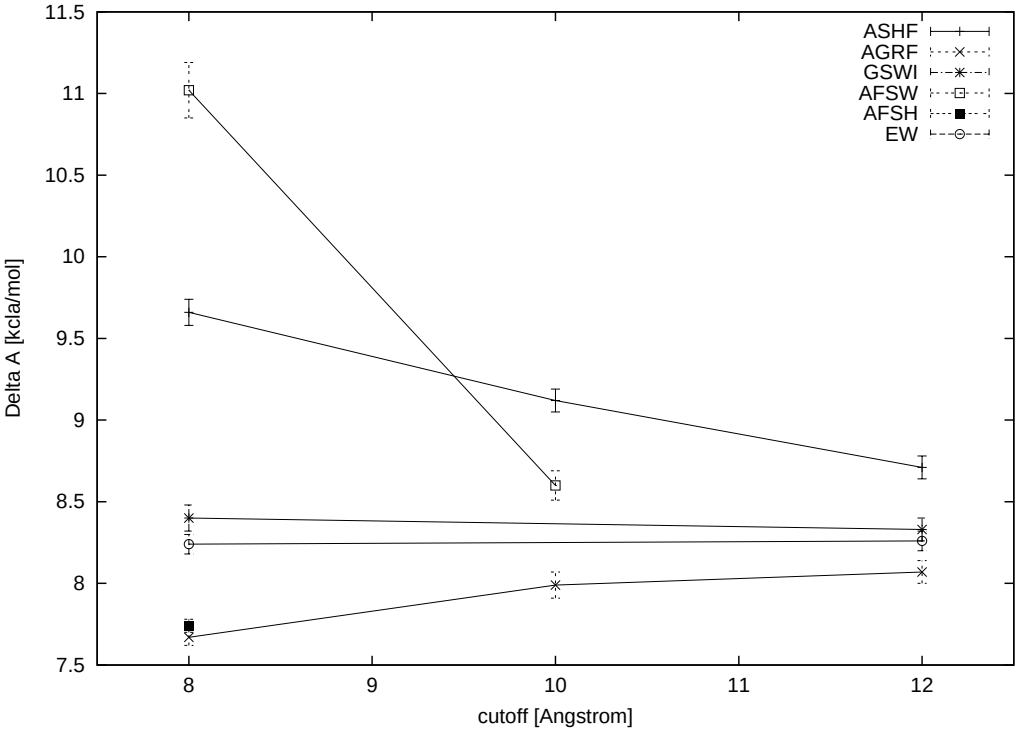

estimates — nearly indistinguishable for EW and GSW and, in addition, agree very well with those reported by Chipot et al. [42]. When adding the average ΔA_{VdW} [††], ΔA_{tot} for EW amounts to 6.51 kcal/mol; for GSWI the result is 6.65 kcal/mol. Both values are very close to the experimental result for the free energy of solvation of water of 6.32 kcal/mol. All the other tapering functions respond more or less strongly to variations of the cutoff radius. The results obtained with an 8 Å cutoff span a range of 3.3 kcal/mol. Using a 12 Å cutoff this range still is 0.63 kcal/mol, i.e., larger than the estimated statistical error of the calculations, since for all our calculations σ, as defined in section 4.2, typically lies between 0.05 and 0.15 kcal/mol and never exceeds 0.2 kcal/mol. For the 8 Å cutoff AFSW

[††]This is assumed to be valid, since the variations of ΔA_{VdW} due to the usage of different methods used for dealing with the long-range interactions are negligible small

Table 20: Electrostatic contribution to the free energy of solvation of water; results for different cutoffs and tapering functions

TF	cutoff [Å]		
	8	10	12
ASHF	9.66 ± 0.07	9.12 ± 0.06	8.71 ± 0.06
AFSW	11.02 ± 0.15	8.60 ± 0.08	—
AFSH	7.74 ± 0.03	7.57 ± 0.31[a]	—
GSWI	8.40 ± 0.07	—	8.33 ± 0.06
AGRF	7.66 ± 0.05	7.99 ± 0.07	8.07 ± 0.06
EW	8.24 ± 0.05	—	8.26 ± 0.06
ref[b]	8.75 ± 0.30	8.82 ± 0.30	8.63 ± 0.30
ref[c]	8.15 ± 0.30	—	—

[a]Last minute result, includes only forward simulations
[b]Kollman, results for cutoffs of 8, 10.5 and 12.5 Å
[c]Kollman, cutoffs as above, results include reaction field correction

gives the worst result. It differs by 2.8 kcal/mol from the EW-result. At a cutoff of 10 Å, however, this difference reduces to 0.25 kcal/mol. Calculations done with with GRF and the AFSH-tapering function, although by far not as wrong as AFSW for the 8 Å cutoff, still need to be done with a cutoff of at least 12 Åor 10 Å, respectively, in order to reduce the error well beneath 0.5 kcal. Overall the worst results are obtained with the ASHF tapering function. Although giving a better result as AFSW for the 8 Å cutoff, its difference to the EW value still is nearly 0.5 kcal/mol, even when using the quite large cutoff of 12 Å. The result calculated with EW can be considered as the reference value. Any discrepancy between the experimental and the computed result can be assumed to be *only* due to shortcomings of the force field, i.e. the TIP3P water model. Thus, when

Table 21: VdW-contribution and total free energy of solvation of water; results for different tapering functions

TF	cutoff	ΔA_{VdW}	ΔA_{tot}
ASHF	8	-1.73 ± 0.08	7.93
ASHF	10	-1.58 ± 0.06	7.54
AFSW	8	-1.85 ± 0.10	9.17
GSWI	8	-1.75 ± 0.07	6.65
AGRF	8	-1.70 ± 0.07	5.96
AGRF	10	-1.76 ± 0.06	6.23
ref[a]	8	-1.92 ± .	6.83
ref[b]	8	-1.86 ± .	6.29
exp[c]		— .	6.32

[a]Kollman
[b]Kollman, results include reaction field correction
[c]experimental value at 298.15 K [40]

judging the results obtained with cutoff and some tapering function, they should be compared to the EW results rather than to the experimental value. The results presented here both support and contradict the conclusions of Ref. [42], concerning the role of the treatment of electrostatic interactions in free energy simulations. Chipot et al. [42] found ΔA_{el} to undergo only marginal changes, over a range of 6.5 to 12.5 Å for the cutoff. This finding was confirmed for the case of the GSWI, but not for any of the other tapering functions investigated here. Although switching a potential seems to be much more severe an inroad on the original coulomb potential than shifting the forces, the superiority of the results obtained with the GSWI tapering function can be explained. The crucial point seems not to be the functional form of the switching or shifting function,

but rather the question if its application is group or atom based. The coulomb potential between charged residues decays with r^{-1}, whereas dipole-dipole interactions are proportional to r^{-3}, that is, they decay much faster than the coulomb potential, resulting in a reduced sensibility to small cutoffs. It has to be stressed that using a group based cutoff will improve the results only if these groups are neutral, i.e., have no net charge. For the water simulations this requirement is fulfilled since naturally one TIP3P molecule is taken as a group. When dealing with groups bearing total charges not equal zero, the original problem is restored.

To round off this section, and to complement the results for water, a couple of additional simulations were carried out for the ethane $\rightarrow$ methanol system as described in section 4.1.2. The free energy difference of the transition was calculated for different TFs. The GSW TF could not be examined for this system since methanol consists of two groups, bearing total partial charges. In this case a group based cutoff leads to absurd results. The finding that, for a cutoff of 8 Å, the results obtained with ASHF and AFSW differ by 2.1 kcal/mol supports the conclusions drawn in the preceding paragraph.

6 Summary

A SSS-potential has been implemented into CHARMM. The correct implementation was tested by calculating free energy differences for non-critical systems. The results thereby obtained, were compared to results computed with PERT, an already established free energy module of CHARMM. After this verification of the code, simulations were carried out to calculate the free energy of solvation of neon in water and of water in water. For both of these systems the VdW endpoint problem arises when TI is carried out together with linear λ-scaling. SSS, on the other hand, was shown to be a very successful approach for free energy calculations complicated by a VdWEP. For all systems and setups investigated here, it proved to be both efficient and accurate. The availability of SSS

in CHARMM is of general interest since free energy calculations complicated by the VdWEP could not, or only with a great loss in performance be carried out with CHARMM up to now. Now a number of quite interesting simulations can be performed with CHARMM for the first time. As could be shown here, SSS facilitates the calculation of "absolute" free energies of solvation. Another example is the calculation of the free energy of solvation of a ligand as an intermediate step in the calculation of "absolute" receptor-ligand affinities.

In addition, the influence of the treatment of the long range interactions on free energy simulations of polar molecules was investigated. It turned out that the calculated free energy differences are definitely affected by the choice of tapering function and cutoff radius. In the model calculations of the hydration free energy of water switching the potential in combination with a group based cutoff was — apart from Ewald — the only method providing consistent results independent of the cutoff radius. This, however, holds only for simulations of groups with a zero net charge. Since especially in biomolecular simulations frequently charged groups, such as in certain amino acid residues, are used, the usage of EW or equivalent methods is strongly recommended in this case. In many papers presenting free energy simulation results calculated without employing EW or comparable methods, no specifications are given whether any and which kind of tapering functions were used. Considering the quite large effects resulting from the usage of commonly used tapering functions, they should be taken into account, especially when claiming good agreement to experimental results, or using the results of the free energy simulations to develop or refine force field parameters.

A The separation shifted potentials in Combination with Smoothing Functions

The separation shifted version of a hybrid potential $u(r,\lambda)$ and its derivatives for a pair of sites, separated by a distance r, have the general form

$$\begin{aligned} u(r,\lambda) &= (1-\lambda)u_i(r,\lambda) + \lambda u_f(r,\lambda) \\ \frac{\partial u(r,\lambda)}{\partial r} &= u_f(r,\lambda) - u_i(r,\lambda) + \frac{\partial u_i(r,\lambda)}{\partial r} + \frac{\partial u_f(r,\lambda)}{\partial r} \\ \frac{\partial u(r,\lambda)}{\partial \lambda} &= u_f(r,\lambda) - u_i(r,\lambda) + \frac{\partial u_i(r,\lambda)}{\partial \lambda} + \frac{\partial u_f(r,\lambda)}{\partial \lambda} \end{aligned}$$

A.1 Coulomb Interactions

A.1.1 unmodified equations

$$\begin{aligned} u_i(r,\lambda) &= \frac{q_i^a\ q_i^b}{(r^2+\delta_e\lambda)^{\frac{1}{2}}} \\ u_f(r,\lambda) &= \frac{q_f^a\ q_f^b}{(r^2+\delta_e(1-\lambda))^{\frac{1}{2}}} \\ \frac{\partial u_i(r,\lambda)}{\partial r} &= -\frac{q_i^a\ q_i^b r}{(r^2+\delta_e\lambda)^{\frac{3}{2}}} \\ \frac{\partial u_f(r,\lambda)}{\partial r} &= -\frac{q_f^a\ q_f^b r}{(r^2+\delta_e(1-\lambda))^{\frac{3}{2}}} \\ \frac{\partial u_i(r,\lambda)}{\partial \lambda} &= -\frac{q_i^a\ q_i^b \lambda}{2(r^2+\delta_e\lambda)^{\frac{3}{2}}} \\ \frac{\partial u_f(r,\lambda)}{\partial \lambda} &= \frac{q_i^a\ q_i^b \lambda}{2(r^2+\delta_e\lambda)^{\frac{3}{2}}} \end{aligned}$$

A.1.2 ASHF

$$\begin{aligned} \mathrm{SHF}(r) &= 1 - 2\frac{r^2}{r_c^2} + \frac{r^4}{r_c^4} \\ \mathrm{DSHF}(r) &= \frac{\partial \mathrm{SHF}(r)}{\partial r} = 4\left(\frac{r^3}{r_c^4} - \frac{r}{r_c^2}\right) \end{aligned}$$

$$
\begin{aligned}
u_i(r,\lambda) &= \mathrm{SHF}(r)\ \frac{q_i^a\ q_i^b}{(r^2+\delta_e\lambda)^{\frac{1}{2}}} \\
u_f(r,\lambda) &= \mathrm{SHF}(r)\ \frac{q_f^a\ q_f^b}{(r^2+\delta_e(1-\lambda))^{\frac{1}{2}}} \\
\frac{\partial u_i(r,\lambda)}{\partial r} &= \mathrm{DSHF}(r)\ \frac{q_i^a\ q_i^b}{(r^2+\delta_e\lambda)^{\frac{1}{2}}} - \mathrm{SHF}(r)\ \frac{q_i^a\ q_i^b r}{(r^2+\delta_e\lambda)^{\frac{3}{2}}} \\
\frac{\partial u_f(r,\lambda)}{\partial r} &= \mathrm{DSHF}(r)\ \frac{q_f^a\ q_f^b}{(r^2+\delta_e(1-\lambda))^{\frac{1}{2}}} - \mathrm{SHF}(r)\ \frac{q_f^a\ q_f^b r}{(r^2+\delta_e(1-\lambda))^{\frac{3}{2}}} \\
\frac{\partial u_i(r,\lambda)}{\partial \lambda} &= -\mathrm{SHF}(r)\ \frac{q_i^a\ q_i^b \lambda}{2(r^2+\delta_e\lambda)^{\frac{3}{2}}} \\
\frac{\partial u_f(r,\lambda)}{\partial \lambda} &= \mathrm{SHF}(r)\ \frac{q_i^a\ q_i^b \lambda}{2(r^2+\delta_e(1-\lambda))^{\frac{3}{2}}}
\end{aligned}
$$

A.1.3 AFSW

$0 \le \mathbf{r} \le \mathbf{r_i}$

$$
\mathrm{SWF}(r) = \frac{(r_c^2-r^2)^2(r_c^2-3r_i^2+2r_2)}{(r_c^2-r_i^2)^3}
$$

$$
\begin{aligned}
u_i(r,\lambda) &= \frac{q_i^a\ q_i^b}{\sqrt{r^2+\delta_e\ \lambda}} + \frac{8\ q_i^a\ q_i^b}{5\ (r_c-r_i)^3\ (r_c+r_i)^3}\ \Big\{(-5\ r_c^2+r_i^2-4\delta_e\lambda) \\
&\quad (r_i^2+\delta_e\ \lambda)^{3/2} + (r_c^2+\delta_e\ \lambda)^{3/2}(-r_c^2+5r_i^2+4\delta_e\lambda)\Big\}
\end{aligned}
$$

$$
\begin{aligned}
u_f(r,\lambda) &= \frac{q_f^a\ q_f^b}{\sqrt{r^2+\delta_e(1-\lambda)}} + \frac{8\ q_f^a\ q_f^b}{5(r_c-r_i)^3(r_c+r_i)^3}\ \Big\{(r_c^2+5r_i^2+4\delta_e(1-\lambda)) \\
&\quad (r_c^2-\delta_e(1-\lambda))^{3/2} + (r_i^2+\delta_e(1-\lambda))^{3/2}(-5r_c^2+r_i^2+4\delta_e(1-\lambda))\Big\}
\end{aligned}
$$

$$
\begin{aligned}
\frac{\partial u_i(r,\lambda)}{\partial r} &= \frac{q_i^a\ q_i^b}{(r_i^2+\delta_e\lambda)^{3/2}} \\
\frac{\partial u_f(r,\lambda)}{\partial r} &= \frac{q_i^a\ q_i^b}{(r_i^2+\delta_e(1-\lambda))^{3/2}} \\
\frac{\partial u_i(r,\lambda)}{\partial \lambda} &= 4\ \delta_e\ q_i^a\ q_i^b\ \Big\{(\sqrt{r_i^2+\delta_e\lambda}\ (3r_c^2+r_i^2+4\ \delta_e\lambda) + \\
&\quad \sqrt{r_c^2+\delta_e\lambda}\ (r_c^2+3r_i^2+4\ \delta_e\lambda))^{-1} - \frac{1}{8\ (r^2+\delta_e\ \lambda)^{3/2}}\Big\}
\end{aligned}
$$

$$\frac{\partial u_f(r,\lambda)}{\partial \lambda} = 4\ \delta_e\ q_f^a\ q_f^b \Big\{ \Big(\sqrt{r_i^2 + \delta_e(1-\lambda)}\ (3r_c^2 + r_i^2 + 4\ \delta_e(1-\lambda)) + \sqrt{r_c^2 + \delta_e(1-\lambda)}\ (r_c^2 + 3r_i^2 + 4\ \delta_e(1-\lambda)) \Big) - \frac{1}{8\ (r^2 + \delta_e(1-\lambda))^{3/2}} \Big\}$$

$\mathbf{r_i \le r \le r_c}$

$$u_i(r,\lambda) = \frac{8\ q_i^a\ q_i^b\ (r_c^2 + \delta_e\ \lambda)^{3/2}(r_c^2 - 5\ r_i^2 - 4\ \delta_e\ \lambda)}{5\ (r_c^2 - r_i^2)^3} 5$$

$$u_f(r,\lambda) = \frac{8\ q_f^a\ q_f^b\ (r_c^2 + \delta_e\ (1-\lambda))^{3/2}(r_c^2 - 5\ r_i^2 - 4\ \delta_e\ (1-\lambda))}{5\ (r_c^2 - r_i^2)^3}$$

$$\frac{\partial u_i(r,\lambda)}{\partial r} = \frac{r\ q_i^a\ q_i^b}{r_c^2 + \delta_e\ \lambda)^{3/2}}\ \mathrm{SWF}(r)$$

$$\frac{\partial u_f(r,\lambda)}{\partial r} = \frac{r\ q_f^a\ q_f^b}{r_c^2 + \delta_e\ (1-\lambda))^{3/2}}\ \mathrm{SWF}(r)$$

$$\frac{\partial u_i(r,\lambda)}{\partial \lambda} = \frac{\delta_e\ q_i^a\ q_i^b}{2\ (r_c^2 - r_i^2)^3} \Big\{ 8\sqrt{r_c^2 + \delta_e\ \lambda}(r_c^2 + 3\ r_i^2 + 4\ \delta_e\lambda) - \frac{1}{(r^2 + \delta_e\ \lambda)^{3/2}} \Big[r_c^6 - 3\ r_c^4\ r_i^2 + 8\ \delta_e^2\ \lambda^2(3\ r_i^2 + 4\ \delta_e\ \lambda) + 12\ \delta_e\lambda(3\ r_i^2 + 4\ \delta_e\ \lambda)\ r^2 + 3\ (3\ r_i^2 + 4\ \delta_e\ \lambda)\ r^4 - 2\ r^6 + 3r_c^2\big(4\ \delta_e\ \lambda(r_i^2 + 2\ \delta_e\ \lambda) + 6\ (r_i^2 + 2\ \delta_e\ \lambda)r^2 + 3\ r^4\big) \Big] \Big\}$$

$$\frac{\partial u_f(r,\lambda)}{\partial \lambda} = \frac{\delta_e\ q_f^a\ q_f^b}{2\ (r_c^2 - r_i^2)^3\ (r_2 + \delta_e\ (1-\lambda))^2} \Big\{ -8\big(r_c^2 + 3\ r_i^2 + 4\ \delta_e\ (1-\lambda)\big)\sqrt{r_c^2 + \delta_e + (1-\lambda)}\ \big(r^2 + \delta_e\ (1-\lambda)\big)^2 + \sqrt{r^2 + \delta_e + (1-\lambda)}\ \Big[r_c^6 - 3\ r_c^4\ r_i^2 + 32\ \delta_e^2(1-\lambda)^3 + 18\ r_c^2\ r_i^2\ r^2 + 9\ (r_c^2 + r_i^2)\ r^4 - 2\ r_6 + 24\ \delta_e^2\ (1-\lambda)^2\ (r_c^2 + r_i^2 + 2\ r^2) + 12\ \delta_e\ (1-\lambda)\ \big(r_c^2\ r_i^2 + 3\ (r_c^2 + r_i^2)\ r_2 + r^4\big) \Big] \Big\}$$

A.1.4 GRF

$$u_i(r,\lambda) = \frac{q_i^a\ q_i^b}{sqrtr_2 + \delta_e\ \lambda}\left(1 - \frac{r}{r_c}\right)^4 \left(1 + \frac{8\ r}{5\ r_c} + \frac{2\ r^2}{5\ r_c^2}\right)$$

$$u_f(r,\lambda) = \frac{q_f^a\ q_f^b}{sqrtr_2 + \delta_e\ (1-\lambda)}\left(1 - \frac{r}{r_c}\right)^4 \left(1 + \frac{8\ r}{5\ r_c} + \frac{2\ r^2}{5\ r_c^2}\right)$$

$$\frac{\partial u_i(r,\lambda)}{\partial r} = \frac{q_i^a\ q_i^b}{5\ r_c^6\ (\delta_e\ \lambda + r^2)^{\frac{3}{2}}}\ (r - r_c)^3\Big(12\ \delta_e\ \lambda(r^2 + 3rr_c + r_c^2) + 5\ r\ (r_c^3 + 3r_c^2 r + 6r_c r^2 + 2r^3)\Big)$$

$$\frac{\partial u_f(r,\lambda)}{\partial r} = \frac{q_f^a\ q_f^b}{5\ r_c^6\ (\delta_e\ (1-\lambda) + r^2)^{\frac{3}{2}}}\ (r - r_c)^3\Big(12\ \delta_e\ (1-\lambda)(r^2 + 3rr_c + r_c^2) + 5\ r\ (r_c^3 + 3r_c^2 r + 6r_c r^2 + 2r^3)\Big)$$

$$\frac{\partial u_i(r,\lambda)}{\partial \lambda} = -\frac{\delta_e\ q_i^a\ q_i^b}{10\ r_c^6\ (\delta_e\ \lambda + r^2)^{\frac{3}{2}}}\ (r - r_c)^4\ (2r^2 + 8rr_c + 5r_c^2)$$

$$\frac{\partial u_f(r,\lambda)}{\partial \lambda} = \frac{\delta_e\ q_f^a\ q_f^b}{10\ r_c^6\ (\delta_e\ (1-\lambda) + r^2)^{\frac{3}{2}}}\ (r - r_c)^4\ (2r^2 + 8rr_c + 5r_c^2)$$

A.1.5 GSWI

Here R is the group-group and r the site-site distance. For $0 \leq r \leq r_i$ the unmodified equations, as given above, are used.

$\mathbf{r_i \leq r \leq r_c}$

$$\mathrm{SWF}(R) = \frac{(r_c^2 - R^2)^2(r_c^2 - 3r_i^2 + 2R_2)}{(r_c^2 - r_i^2)^3}$$

$$\mathrm{DSWF}(R) = 12\ R\ (r_c^2 - R^2)(r_i^2 - R^2)/(r_c^2 - r_i^2)^3$$

$$u_i(r,R,\lambda) = \mathrm{SWF}(R)\frac{q_i^a\ q_i^b}{\sqrt{r^2 + \delta_e\ \lambda}}$$

$$u_f(r,R,\lambda) = \mathrm{SWF}(R)\frac{q_f^a\ q_f^b}{\sqrt{r^2+\delta_e\ (1-\lambda)}}$$

$$\frac{\partial u_i(r,R,\lambda)}{\partial r} = \mathrm{DSWF}(R)\frac{q_i^a\ q_i^b}{\sqrt{r^2+\delta_e\ \lambda}} - \mathrm{SWF}(R)\frac{q_i^a\ q_i^b\ r}{(r^2+\delta_e\ \lambda)^{\frac{3}{2}}}$$

$$\frac{\partial u_f(r,R,\lambda)}{\partial r} = \mathrm{DSWF}(R)\frac{q_f^a\ q_f^b}{\sqrt{r^2+\delta_e\ (1-\lambda)}} - \mathrm{SWF}(R)\frac{q_f^a\ q_f^b\ r}{(r^2+\delta_e\ (1-\lambda))^{\frac{3}{2}}}$$

$$\frac{\partial u_i(r,R,\lambda)}{\partial \lambda} = -\mathrm{SWF}(R)\frac{q_i^a\ q_i^b\ \delta_e}{2\ (r^2+\delta_e\ \lambda)^{\frac{3}{2}}}$$

$$\frac{\partial u_f(r,R,\lambda)}{\partial \lambda} = \mathrm{SWF}(R)\frac{q_f^a\ q_f^b\ \delta_e}{2\ (r^2+\delta_e\ (1-\lambda))^{\frac{3}{2}}}$$

A.2 VdW Interactions

A.2.1 unmodified equations

$$u_i(r,\lambda) = 4\ \epsilon_i\left(\frac{\sigma_i^{12}}{(r^2+\delta_v\lambda)^6} - \frac{\sigma_i^6}{(r^2+\delta_v\lambda)^3}\right)$$

$$u_f(r,\lambda) = 4\ \epsilon_f\left(\frac{\sigma_f^{12}}{(r^2+\delta_v\lambda)^6} - \frac{\sigma_f^6}{(r^2+\delta_v\lambda)^3}\right)$$

$$\frac{\partial u_i(r,\lambda)}{\partial r} = 4\ \epsilon_i\ r\ \left(-\frac{12\ \sigma_i^{12}}{(r^2+\delta_v\lambda)^7} + \frac{6\ \sigma_i^6}{(r^2+\delta_v\lambda)^4}\right)$$

$$\frac{\partial u_f(r,\lambda)}{\partial r} = 4\ \epsilon_f\ r\ \left(-\frac{12\ \sigma_f^{12}}{(r^2+\delta_v\lambda)^7} + \frac{6\ \sigma_f^6}{(r^2+\delta_v\lambda)^4}\right)$$

$$\frac{\partial u_i(r,\lambda)}{\partial \lambda} = 4\ \epsilon_i\ \delta_v\ \left(-\frac{6\ \sigma_i^{12}}{(r^2+\delta_v\lambda)^7} + \frac{3\ \sigma_i^6}{(r^2+\delta_v\lambda)^4}\right)$$

$$\frac{\partial u_f(r,\lambda)}{\partial \lambda} = 4\ \epsilon_f\ \delta_v\ \left(-\frac{6\ \sigma_f^{12}}{(r^2+\delta_v\lambda)^7} + \frac{3\ \sigma_f^6}{(r^2+\delta_v\lambda)^4}\right)$$

A.2.2 ASWI

For $0 \leq r \leq r_i$ the unmodified equations, as given above, are used.

$\mathbf{r_i \leq r \leq r_c}$

$$\mathrm{SWF}(r) = \frac{(r_c^2 - r^2)^2(r_c^2 - 3r_i^2 + 2r_2)}{(r_c^2 - r_i^2)^3}$$

$$\mathrm{DSWF}(r) = 12\ r\ (r_c^2 - r^2)(r_i^2 - r^2)/(r_c^2 - r_i^2)^3$$

$$u_i(r,\lambda) = swf(r)\ 4\ \epsilon_i \left(\frac{\sigma_i^{12}}{(r^2 + \delta_v\lambda)^6} - \frac{\sigma_i^6}{(r^2 + \delta_v\lambda)^3} \right)$$

$$u_f(r,\lambda) = swf(r)\ 4\ \epsilon_f \left(\frac{\sigma_f^{12}}{(r^2 + \delta_v\lambda)^6} - \frac{\sigma_f^6}{(r^2 + \delta_v\lambda)^3} \right)$$

$$\frac{\partial u_i(r,\lambda)}{\partial r} = \mathrm{SWF}(r)\ 4\ \epsilon_i\ r \left(- \frac{12\ \sigma_i^{12}}{(r^2 + \delta_v\lambda)^7} + \frac{6\ \sigma_i^6}{(r^2 + \delta_v\lambda)^4} \right) + \mathrm{DSWF}(r)\ 4\ \epsilon_i \left(\frac{\sigma_i^{12}}{(r^2 + \delta_v\lambda)^6} - \frac{\sigma_i^6}{(r^2 + \delta_v\lambda)^3} \right)$$

$$\frac{\partial u_f(r,\lambda)}{\partial r} = \mathrm{SWF}(r)\ 4\ \epsilon_f\ r \left(- \frac{12\ \sigma_f^{12}}{(r^2 + \delta_v\lambda)^7} + \frac{6\ \sigma_f^6}{(r^2 + \delta_v\lambda)^4} \right) + \mathrm{DSWF}(r)\ 4\ \epsilon_f \left(\frac{\sigma_f^{12}}{(r^2 + \delta_v\lambda)^6} - \frac{\sigma_f^6}{(r^2 + \delta_v\lambda)^3} \right)$$

$$\frac{\partial u_i(r,\lambda)}{\partial \lambda} = \mathrm{SWF}(r)\ 4\ \epsilon_i\ \delta_v \left(- \frac{6\ \sigma_i^{12}}{(r^2 + \delta_v\lambda)^7} + \frac{3\ \sigma_i^6}{(r^2 + \delta_v\lambda)^4} \right)$$

$$\frac{\partial u_f(r,\lambda)}{\partial \lambda} = \mathrm{SWF}(r)\ 4\ \epsilon_f\ \delta_v \left(- \frac{6\ \sigma_f^{12}}{(r^2 + \delta_v\lambda)^7} + \frac{3\ \sigma_f^6}{(r^2 + \delta_v\lambda)^4} \right)$$

References

[1] N. Metropolis *et al.*, J. Chem. Phys. **21**, 1087 (1953).

[2] B. J. Alder and T. E. Wainwright, J. Chem. Phys. **27**, 1208 (1957).

[3] M. Zacharias, T. P. Straatsma, and J. A. McCammon, J. Chem. Phys. **100**, 9025 (1994).

[4] T. C. Beutler, A. E. Mark, R. C. van Schaik, and P. R. Gerber, Chem. Phys. Lett. **222**, 529 (1994).

[5] B. R. Brooks *et al.*, J. Comput. Chem. **4**, 187 (1983), the respective latest version of the all-atom force-field by Alex D. MacKerell Jr. *et al.* is included with the current version of the program.

[6] G. Hummer, D. M. Soumpasis, and M. Neumann, J. Phys.: Condens. Matter **6**, A141 (1994).

[7] T. L. Hill, *Statistical thermodynamics* (Addison-Wesley, Reading, Massachusits, 1960).

[8] D. McQuarrie, *Statistical thermodynamics* (Harper& Row, New York, 1973).

[9] W. G. Hoover, Phys. Rev. **A31**, 1695 (1985).

[10] A. Ben-Naim, *Statistical Thermodynamics for Chemists and Biochemists* (Plenum Press, New York, London, 1992).

[11] D. L. Beveridge and F. M. DiCapua, in *Computer Simulation of Molecular Systems*, edited by W. F. van Gunsteren and P. K. Weiner (ESCOM Science Publishers B. V., Leiden, NL, 1989), pp. 1–25.

[12] R. W. Zwanzig, J. Chem. Phys. **22**, 1420 (1954).

[13] J. G. Kirkwood and B. J. Alder, *Theory of Liquids* (Gordon and Breach, New York, 1968).

[14] J. G. Kirkwood, J. Chem. Phys. **3**, 300 (1935).

[15] P. A. K. D. A. Pearlman, J. Chem. Phys. **91**, 7831 (1989).

[16] M. R. Reddy and M. D. Erion, J. Comp. Chem. **20**, 1018 (1999).

[17] A. J. Cross, Chem. Phys. Lett. **128**, 198 (1986).

[18] J. Schlitter, Molecular Simulation **7**, 105 (1990).

[19] T. Simonson, Molecular Physics **80**, 441 (1993).

[20] G. M. Torrie and J. P. Valleau, Chem. Phys. Lett. **28**, 578 (1974).

[21] N. Nakajima, H. Nakamura, and A. Kidera, J. Phys. Chem. B **101**, 817 (1997).

[22] R. M. Shroll and D. E. Smith, J. Chem. Phys. **110**, 8295 (1999).

[23] P. Kollman, Chem. Rev. **93**, 2395 (1993).

[24] M. P. Allen and D. J. Tildesley, *Computer simulations of liquids* (Oxford University Press, New York, 1989).

[25] P. J. Steinbach and B. R. Brooks, J. Comp. Chem. **15**, 667 (1994).

[26] M. Neumann, J. Chem. Phys. **82**, 5663 (1985).

[27] A. Y. Toukmaji and J. A. Board, Jr., Comp. Phys. Comm. **95**, 73 (1996).

[28] D. Fincham, Molec. Sim. **13**, 1 (1994).

[29] D. J. Adams and G. S. Durey, J. Comp. Phys. **72**, 156 (1986).

[30] R. Abseher, H. Schreiber, and O. Steinhauser, Proteins **25**, 366 (1996).

[31] S. Boresch and O. Steinhauser, Ber. Bunsenges. Phys. Chem. **101**, 1019 (1997).

[32] S. Boresch and M. Karplus, J. Phys. Chem. A **103**, 103 (1999).

[33] I. Wolfram Research, *Mathematica, Version 3.0*, version 3.0 ed. (Wolfram Research, Inc., Champaign, Illinois, 1996).

[34] W. L. Jorgensen and C. J. Ravimohan, Chem. Phys. **83**, 3050 (1985).

[35] T. Simonson and A. T. Brünger, Biochemistry **31**, 8661 (1992).

[36] G. P. Brady and F. A. Sharp, J. Mol. Biol. **245**, 77 (1995).

[37] E. Neria, S. Fischer, and M. Karplus, J. Chem. Phys. **105**, 1902 (1996).

[38] P. Höchtl, S. Boresch, W. Bitomsky, and O. Steinhauser, J. Chem. Phys. **109**, 4927 (1998).

[39] S. Boresch and M. Karplus, J. Phys. Chem. A **103**, 119 (1999).

[40] A. Ben-Naim and Y. J. Marcus, J. Chem. Phys. **81**, 2016 (1984).

[41] F. Franks and D. S. Reid, in *Water, A Comprehensive Treatise*, edited by F. Franks (Plenum, New York, 1973), p. 323.

[42] C. Chipot, C. Millot, B. Maigret, and P. A. Kollman, J. Chem. Phys. **101**, 7953 (1994).

Lebenslauf

17.04.1970	Geboren in Gmunden, Oberösterreich
1976-1980	Volsschule, Vöcklabruck, Oberösterreich
1971-1988	Neusprachliches Gymnasium, Vöcklabruck
1988-1989	Studium der vergleichenden Literaturwissenschaften, Universität Wien
1989-1991	Studium der Chemie, Universität Wien
1992-1995	Studium der Lebensmittel- und Biotechnologie, Universität f. Bodenkultur Wien
1995-1999	Individuelles Diplomstudium (Biotechnologie und computative Biochemie), Universität f. Bodenkultur, Universität Wien
Dez. 1998	Beginn der Diplomarbeit am Institut für theoretische Chemie (Univ. Wien), Betreuer: Prof O. Steinhauser (Univ. Wien), Prof. J. Fischer (BOKU),